Decadal Modulations of Interhemispheric Global Atmospheric Circulations and Monsoons by the South Atlantic Meridional Overturning Circulation

HOSMAY LOPEZ, SHENFU DONG, AND SANG-KI LEE

Cooperative Institute for Marine and Atmospheric Studies, University of Miami, and NOAA/Atlantic Oceanographic and Meteorological Laboratory, Miami, Florida

GUSTAVO GONI

NOAA/Atlantic Oceanographic and Meteorological Laboratory, Miami, Florida

(Manuscript received 17 July 2015, in final form 13 November 2015)

ABSTRACT

This study presents a physical mechanism on how low-frequency variability of the South Atlantic meridional heat transport (SAMHT) may influence decadal variability of atmospheric circulation. A multicentury simulation of a coupled general circulation model is used as basis for the analysis. The highlight of the findings herein is that multidecadal variability of SAMHT plays a key role in modulating global atmospheric circulation via its influence on interhemispheric redistributions of momentum, heat, and moisture. Weaker SAMHT at 30°S produces anomalous ocean heat divergence over the South Atlantic, resulting in negative ocean heat content anomalies about 15–20 years later. This forces a thermally direct anomalous interhemispheric Hadley circulation, transporting anomalous atmospheric heat from the Northern Hemisphere (NH) to the Southern Hemisphere (SH) and moisture from the SH to the NH, thereby modulating global monsoons. Further analysis shows that anomalous atmospheric eddies transport heat northward in both hemispheres, producing eddy heat flux convergence (divergence) in the NH (SH) around 15°–30°, reinforcing the anomalous Hadley circulation. The effect of eddies on the NH (SH) poleward of 30° depicts heat flux divergence (convergence), which must be balanced by sinking (rising) motion, consistent with a poleward (equatorward) displacement of the jet stream. This study illustrates that decadal variations of SAMHT could modulate the strength of global monsoons with 15–20 years of lead time, suggesting that SAMHT is a potential predictor of global monsoon variability. A similar mechanistic link exists between the North Atlantic meridional heat transport (NAMHT) at 30°N and global monsoons.

1. Introduction

The Atlantic meridional overturning circulation (AMOC) is characterized by northward-flowing warm water in the upper ocean and a southward compensating flow of cold water at depth (e.g., Broecker 1991; Lumpkin and Speer 2007). There have been numerous efforts to understand the role of the AMOC as a potential predictor of decadal climate variability, motivated partly by its inherent relationship with the North Atlantic sea surface temperature (SST; e.g., Latif et al. 2006; Corti et al. 2012). Therefore, the majority of efforts to understand the dynamics of the AMOC and its climate impacts have focused on the North Atlantic. The mechanism for the North Atlantic multidecadal SST variability, also known as the Atlantic multidecadal oscillation (AMO; e.g., Enfield et al. 2001), has been shown to be modulated by AMOC changes (e.g., Latif et al. 2004; Knight et al. 2005; Zhang and Wang 2013) and linked to decadal variability of the North Atlantic Oscillation (NAO; e.g., Sun et al. 2015b).

Sun et al. (2015b) suggested a three-way interaction among the NAO, AMOC, and AMO with the NAO leading the AMO by 15–20 years, with the AMO providing a delayed negative feedback to the NAO. Latif et al. (2000) also found a similar relationship between decadal variability of the NAO and North Atlantic SSTs. Drévillon et al. (2001) argued that SST anomalies over the North Atlantic induce atmospheric stationary waves, which

Corresponding author address: Hosmay Lopez, UM/CIMAS/RSMAS and NOAA/AOML/PHOD, 4301 Rickenbacker Causeway, Miami, FL 33149.
E-mail: hlopez@rsmas.miami.edu

DOI: 10.1175/JCLI-D-15-0491.1

are strengthened by transient eddies. These studies collectively showed that the AMO influences and also is influenced by the strength of the AMOC and associated meridional heat transport (MHT), suggesting a delayed advective oscillation (Lee and Wang 2010).

North Atlantic SST anomalies associated with the AMO significantly influence climate anomalies over North America, West Africa, and Europe (e.g., Enfield et al. 2001; Kushnir et al. 2002; Rodwell and Folland 2003; Knight et al. 2006; Zhang and Delworth 2006; Ting et al. 2011; Tung and Zhou 2013; Peings and Magnusdottir 2014). Several studies have suggested that the AMO's impact on climate is largely forced in the low latitudes (e.g., Sutton and Hodson 2005). By modulating the strength and meridional location of the Atlantic intertropical convergence zone (ITCZ), the AMO can force extratropical atmospheric stationary waves to influence summertime western Europe temperature anomalies (Ambrizzi et al. 1995; Cassou et al. 2004; Cassou et al. 2005). Some studies argue that the meridional ITCZ shifts are also linked to sea ice concentrations over the North Atlantic (Chiang and Bitz 2005), freshwater fluxes into the North Atlantic (Stouffer et al. 2006; Zhang and Delworth 2005), and aerosol-induced heating or cooling over the high latitudes in the Northern Hemisphere (NH) (e.g., Yoshimori and Broccoli 2008). Kang et al. (2009) proposed that antisymmetric interhemispheric heating in high latitudes linked to AMOC shutdown could control the location of the ITCZ, and that its shift could be related to changes in atmospheric energy transport. Consistently, Frierson et al. (2013) argued that oceanic MHT contributes significantly to the asymmetry in precipitation by transporting heat northward, which moves the tropical rainband and ITCZ northward. Several studies argue for the existence of two stable AMOC states, an ''on'' and an ''off'' state, from theoretical arguments (Stommel 1961), modeling studies (Manabe and Stouffer 1988; Lenton et al. 2009; Hawkins et al. 2011), and paleoclimate records (Broecker et al. 1985; Clark et al. 2002). Recent numerical model twenty-first-century projections suggest a considerable weakening of the AMOC (Kriegler et al. 2009; Cheng et al. 2013). Zhang and Delworth (2005) showed that a substantial weakening of the AMOC results in a southward shift of the ITCZ, with a weakening of the Indian and Asian summer monsoons, and an El Niño–like pattern in the southeastern Pacific.

As briefly reviewed above, the majority of efforts to understand the dynamics of the AMOC and its climate impact are focused on the North Atlantic. Recently, the research community started investigating and assessing the role of the South Atlantic on climate. Direct or indirect measurements from in situ observations have shown a wide range of AMOC values at 35°S from −0.24 PW (de las Heras and Schlitzer 1999) to 0.55 PW (Dong et al. 2011a) and to 0.94 PW (Saunders and King 1995). The AMOC over the South Atlantic Ocean is unique in that it is the only major ocean basin that transports heat from the pole toward the equator (Talley 2003). Recent studies have suggested the possibility of the anomalous AMOC and MHT originating from the interocean transport from the Indian Ocean (e.g., Biastoch et al. 2009; Lee et al. 2011).

The South Atlantic Ocean is characterized by complex and unique ocean dynamic processes, which are important to the global distribution of energy. For example, the Malvinas–Brazil Confluence (Garzoli and Garraffo 1989; Goni et al. 2011) plays a critical role in the exchange of water masses between the subpolar and the subtropical regions. The Agulhas leakage, which is the main balance for the outflow of North Atlantic Deep Water (Gordon 1985; Sloyan and Rintoul 2001), has the potential for modifying the long-term AMOC response, which could impact global atmospheric circulation and climate (Sloyan and Rintoul 2001; Garzoli and Matano 2011). Dong et al. (2011b) pointed out that interannual and longer-term decadal changes in AMOC and MHT over the South Atlantic are due to advective heat convergence from interbasin heat exchange, mainly through the Agulhas leakage. Lee et al. (2011) showed that this interbasin heat transport has increased since the 1950s and contributed to the significant increase in Atlantic Ocean heat content.

Here, we present a physical mechanism by which the South Atlantic meridional heat transport (SAMHT) modulates changes in the atmospheric circulation. Our hypothesis is that low-frequency variations in SAMHT influence interhemispheric atmospheric heat and moisture transport through slow changes in the upper ocean heat content of the South Atlantic. Our study shows that this upper ocean heat content anomaly, linked to meridional heat convergence and divergence, forces a thermally direct anomalous interhemispheric Hadley circulation as well as atmospheric eddy-driven circulations in both hemispheres, and thus shifts the location and strength of the ITCZ and modulates monsoonal circulations.

The motivation of this work is to enhance our understanding of the SAMHT and its potential role in predicting global and regional climate variability. In this work, we show that a weaker-than-normal SAMHT leads to a strengthening and northward shift of the ITCZ about 15–20 years later. This is possible through a modification of the zonal mean atmospheric Hadley circulation by anomalous negative heat content over the tropical

South Atlantic, with potential implications for the global monsoon circulations. For this, multicentury output from a coupled general circulation model (CGCM) is analyzed. Basic information about the model is presented in section 2. Multidecadal variability of the Atlantic Ocean transports is discussed in section 3. Section 4 discusses the atmospheric response to changes in SAMHT. Section 5 presents the SAMHT modulation of precipitation and monsoon circulations. Section 6 investigates the relative roles of SAMHT and the North Atlantic MHT (NAMHT). A summary is presented in section 7, with discussion of a possible mechanism for multidecadal ocean–atmosphere interactions. Conclusions are presented in section 8.

2. Data and coupled model

The global estimate of precipitation for the period from January 1950 to December 2011 is taken from the Global Precipitation Climatology Centre (GPCC; Becker et al. 2013) on a 1° grid. Estimates for the AMOC and MHT at 26°N are from direct measurements from the Rapid Climate Change Meridional Overturning Circulation and Heat Flux Array (RAPID-MOCHA) observing system (Cunningham et al. 2007). The estimates of the MHT at 34°S are derived from expendable bathythermograph (XBT) and Argo float measurements (Dong et al. 2009, 2014).

The CGCM used in this work is the Community Earth System Model, version 1 (CESM1), from the National Center for Atmosphere Research (NCAR). This earth system model consists of atmosphere, land, ocean, glaciers, and sea ice components, all linked by a flux coupler. The coupler exchanges daily information among the components interactively. The atmospheric component is the Community Atmosphere Model, version 5 (CAM5). It has 30 vertical levels with horizontal resolution of 1.25° longitude by 0.94° latitude. The dynamical core uses the finite volume formulation. It employs an improved deep convection scheme by inclusion of subgrid convective momentum transport and a more realistic dilution approximation for the calculation of convective available potential energy (Neale et al. 2008). The ocean model component uses the Parallel Ocean Program, version 2 (POP2; Danabasoglu et al. 2012). It has a 1° horizontal resolution with 60 vertical levels. This updated version of POP includes a simplified version of the near boundary eddy flux parameterization of Ferrari et al. (2008), vertically varying isopycnal diffusivity coefficients (Danabasoglu and Marshall 2007), an abyssal tidally driven mixing parameterization, modified anisotropic horizontal viscosity coefficients (Jochum et al. 2008), and a modified *K*-profile parameterization with horizontally varying background vertical diffusivity and viscosity coefficients (Jochum 2009).

An extensive evaluation of the ocean component of the model over the South Atlantic and Southern Ocean was discussed in Weijer et al. (2012). There, they showed that simulated ocean variability over the Southern Hemisphere (SH) is dominated by the southern annular mode, which is consistent with observations. The model also reproduces the correct characteristics of the frontal zone associated with the Antarctic Circumpolar Current and the SH interbasin ocean exchanges to a reasonable degree. However, the model struggles in representing the correct location of the Brazil–Malvinas Current Confluence, which is displaced southward compared to observations. Also, the Agulhas leakage is too strong, and is zonally oriented compared to satellite observational estimates.

To have a robust estimate of the mean climate and variability, we evaluate 1100 years of preindustrial simulation using CESM1. More detailed discussions on this model can be found in Kay et al. (2015). All choices of fields analyzed are from monthly mean model outputs. Although the model does not show any long-term climate drift, all data are detrended before analysis. The model run is a preindustrial simulation with atmospheric composition from 1850, since we are mainly interested in internal variability in this study.

3. Results

a. South Atlantic meridional heat transport

Figure 1 shows the mean ocean MHT in the Atlantic derived from CESM1 and from various observational and reanalysis products. The mean MHT over the Atlantic Ocean is well represented in CESM1. Its amplitude is larger than estimates from the European Centre for Medium-Range Weather Forecasts (ECMWF) reanalysis and comparable with that derived from the National Centers for Environmental Prediction (NCEP) reanalysis (Trenberth and Caron 2001). Trenberth and Caron (2001) found that ocean MHT estimates from NCEP were in good agreement with direct ocean measurements and coupled models. In contrast, the ECMWF-derived MHT estimates are deficient due to problems with changes in the observing system, specifically satellite data. The mean MHT of 1.18 PW at 26°N from CESM1 is comparable with the 1.33 PW estimated from the RAPID-MOCHA observing system (Johns et al. 2011). The observationally based MHT estimate at 34°S (e.g., Dong et al. 2009, 2015) is also well captured by CESM1. Overall, the MHT over the Atlantic Ocean is well represented by the model.

An index for the SAMHT is constructed here by computing the anomalous MHT across the Atlantic basin at

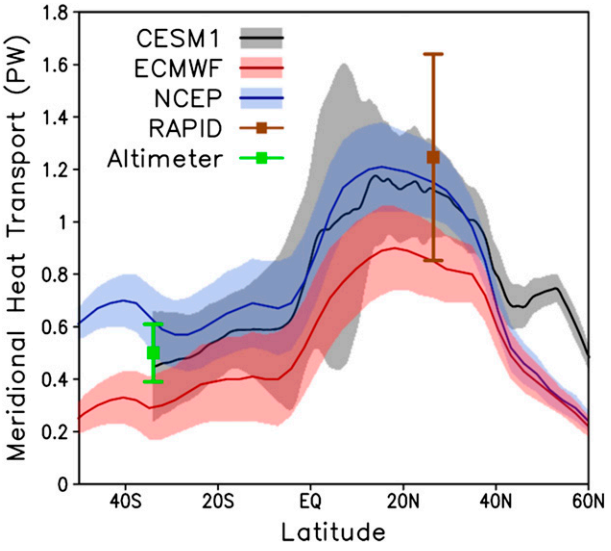

FIG. 1. MHT over the Atlantic Ocean (PW) from CESM1 model (black), gray shading represents one standard deviation. Also shown are estimated transports from NCEP (blue) and ECMWF reanalysis (red) from Trenberth and Caron (2001). Direct estimates from the RAPID array at 26°N are shown in brown. Transport estimates from Argo, XBTs, and altimetry observations at 34°S are shown by green color. The color shading and vertical bars depict one standard deviation calculated from annual average of MHT for each latitude.

30°S, where the anomaly is obtained by removing the seasonal cycle of the transport and any trend that might be present. The SAMHT is further decomposed into the Ekman and geostrophic components. The Ekman component is estimated using monthly mean zonal wind stress from CESM1, whereas the geostrophic term is simply taken as the difference between the total and Ekman component.

There are two dominant power spectral peaks at frequencies of about 30 and 60 yr in the simulated MHT (not shown). In general, the power spectrum of SAMHT is dominated by low frequencies with a red-spectrum structure. The reddening is mostly from the geostrophic component, where most of the power occurs on multidecadal time scales. The Ekman component has power at almost all frequencies, although the 60-yr spectral peak is also prominent there. The multidecadal frequencies (i.e., periods higher than 11 yr) contain about 53% of the total SAMHT variance. For the Ekman (geostrophic) component, the variance explained by the multidecadal frequencies accounts for about 35% (83%) of its total variance. Therefore, it is appropriate to focus on the low-frequency variability of SAMHT. For this, an 11-yr running average is performed on the interannual anomaly of SAMHT, and shown in Fig. 2 as the time series for each component for the 1100 model years. Note that the Ekman and geostrophic components have about the same amplitude as the total SAMHT. Overall, the geostrophic component explains most of the low-frequency variance of the total SAMHT, consistent with the spectral peaks mentioned earlier. It is also evident that the geostrophic component tends to redden the spectrum of the total SAMHT, whereas the Ekman is comprised of higher frequencies, even after the 11-yr running average is applied. The results presented here are largely independent of the choice of the filtering window used, which ranges from 7 to 15 years.

The time series shown in Fig. 2a is used in this work as the basis for studying the relationships between the SAMHT and global climate variability. Those relationships will be assessed via composite analyses of the state of the SAMHT. A strong (weak) SAMHT is defined as periods where SAMHT is one standard deviation above (below) the mean value. Here, a reliable composite difference (i.e., weak minus strong SAMHT) is built from the large sample size.

b. *Ocean transport*

Figure 3 shows the mean and composite difference of the ocean meridional overturning streamfunction for the Atlantic Ocean and the global ocean (positive streamfunction values indicate clockwise circulations). Recall that the composite difference is defined by weak minus strong SAMHT and referred to here as anomaly. For the AMOC (Fig. 3, top), the simulated AMOC is dominated by northward flow in the upper 1000 m and a return flow below. The maximum streamfunction occurs at about 40°N. The anomalous AMOC (Fig. 3, top) indicates that a reduction in SAMHT is accompanied by a significant weakening of the AMOC extending from the South Atlantic to about 45°N. The weakening in the AMOC peaks in two regions, one at 30°S and the other at about 30°N. For the global ocean (Fig. 3, bottom), the largest value of meridional overturning circulation (MOC) also occurs at around 40°N at 1000-m depth. The upper 700-m tropical band (30°S–30°N) is dominated by the shallow overturning cell with upward flow near the equator, occurring predominantly in the Pacific Ocean (Klinger and Marotzke 2000; McPhaden and Zhang 2002, 2004). The anomalous overturning circulation of the global ocean is very similar in amplitude and location to that of the Atlantic, suggesting that the Atlantic basin dominates most of the anomalies at the multidecadal time scales presented here.

c. *Oscillatory mechanism*

This section presents a possible mechanism by which decadal changes in the South Atlantic MOC and associated SAMHT could interplay with atmospheric circulation. For

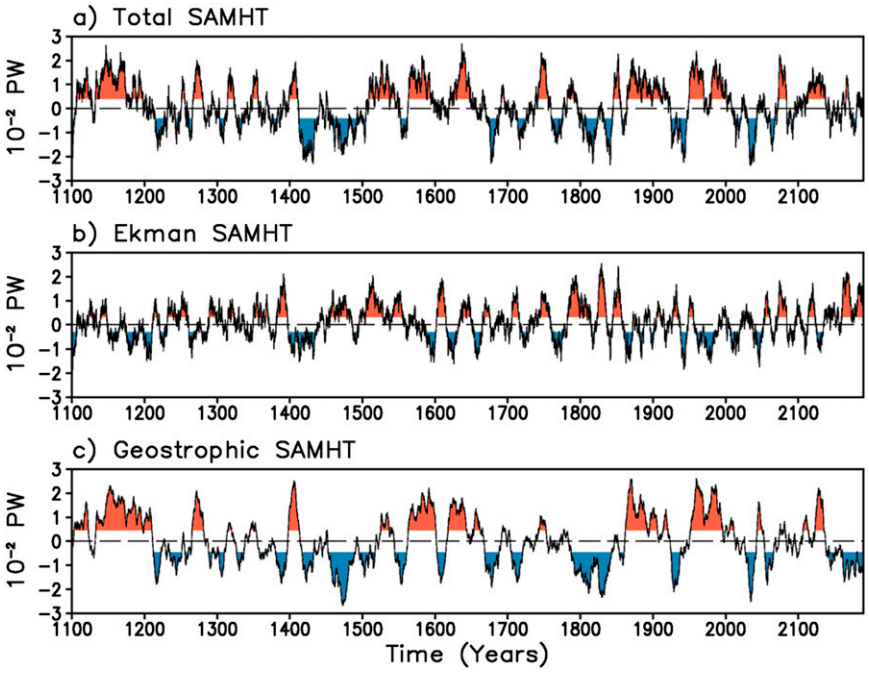

FIG. 2. The 11-yr running average of the SAMHT time series for (a) total, (b) Ekman, and (c) geostrophic component for the 1100 model years analyzed. The total time series is defined as the MHT at 30°S after removing the seasonal cycle and linear trend. The Ekman component is estimated using monthly mean zonal wind stress from CESM1, whereas the geostrophic term is simply taken as the difference between the total and Ekman component. The red (blue) line fill contours indicate values greater (less) than one standard deviation.

this, we analyze the composite difference of Atlantic Ocean MHT, heat content (HC), heat content tendency, MHT divergence, and heat flux as a function of lead time with respect to SAMHT. Figure 4a shows the lead–lag composite difference of Atlantic MHT with respect to weak minus strong SAMHT. Figures 4b–e are similar to Fig. 4a but for the surface–700 m integrated HC, HC tendency, MHT divergence, and surface heat flux in the Atlantic Ocean. Several depths ranging from 200 m down to the ocean bottom were tested to conclude that results shown here are largely independent of the choice of the integration depth for heat content calculation. There is an oscillatory pattern in the MHT (Fig. 4a) that appears to propagate from the north to the south, with North Atlantic MHT leading SAMHT by about 10 yr. That is, the anomalous negative SAMHT can be traced back to the North Atlantic. Interestingly, the SAMHT leads the opposite sign in the North Atlantic MHT by about 15 yr. Overall, the oscillatory pattern has a period of about 50–60 yr.

By construction of the composite, the SAMHT has the most negative value at 0-yr lag. This is associated with a negative tendency of HC from 30°S to the equator (Fig. 4c), which leads the negative HC anomaly 10–20 years later (Fig. 4b). The periods during and after the weakest SAMHT (e.g., 10–20-yr lead) are dominated by negative (positive) HC anomaly over the SH (NH). [The relationship between MHT and HC is described by (1).] Assuming a perfectly enclosed basin, the zonally and vertically integrated tendency in the heat content is balanced by MHT convergence and surface heat fluxes:

$$\frac{\partial \mathrm{HC}}{\partial t} = -\frac{\partial \mathrm{MHT}}{\partial y} + Q_{\mathrm{Net}}, \qquad (1)$$

where the first term on the right is the convergence of the MHT. The second term is the net surface heat flux, the sum of two turbulent (latent and sensible) and two radiative (longwave and shortwave) components. The results described in Fig. 4 show an oscillatory pattern in HC over the South Atlantic (i.e., Fig. 4b) in association with SAMHT. The negative HC tendency at 0-yr lag (Fig. 4c) is mainly caused by MHT divergence south of the equator (Fig. 4d). MHT convergence is balanced by heat content tendency at about 10 years prior to the weakest SAMHT between 15° and 35°N, leading to a positive HC anomaly over most of the North Atlantic at 0-yr lag during the weakest SAMHT. The HC anomaly in the North Atlantic Ocean is explained by MHT convergence, which is balanced by negative surface heat flux at about 10 years prior to the weakest SAMHT. The MHT convergence is mostly balanced by the positive tendency

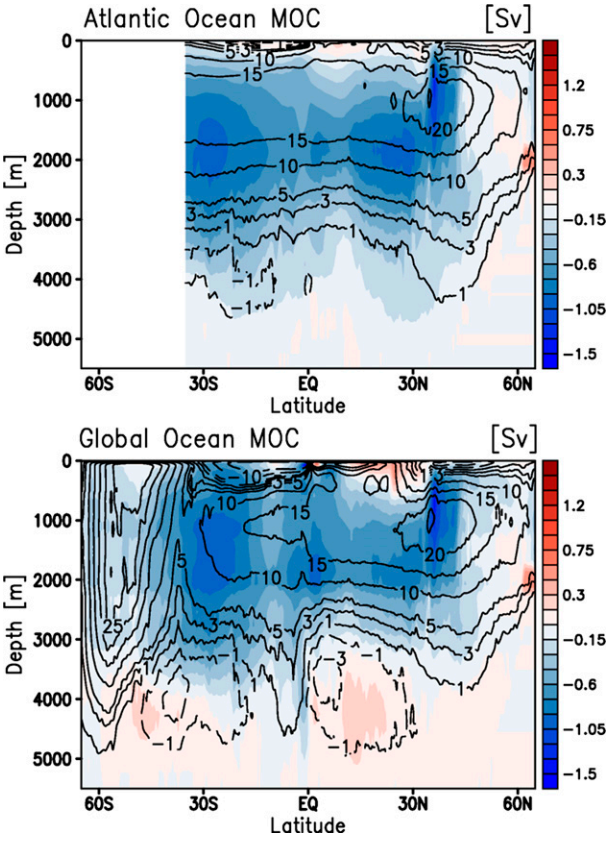

FIG. 3. The mean ocean meridional overturning streamfunction (Sv; 1 Sv $\equiv 10^6\,m^3\,s^{-1}$) for the (top) Atlantic Ocean and (bottom) global ocean, where positive streamfunction indicates clockwise flow. The mean circulation is taken as the time mean, whereas the anomalous circulation is defined by the composite difference between weak minus strong SAMHT, shown by color shading.

of HC. The North Atlantic HC anomaly appears to be modulated by the same physical mechanism explained for the South Atlantic HC anomaly. This relationship among ocean heat content tendency, meridional heat transport convergence, and surface heat fluxes produces the meridional asymmetry in the heat content. Its impact on interhemispheric atmospheric circulation is discussed next.

Anomalous Hadley circulation corresponding to weak minus strong SAMHT is depicted in Fig. 5 as the vertically integrated mass streamfunction about the equator. Here, the direction of interhemispheric atmospheric heat transport is proportional to the mass transport with northward (southward) transport labeled red (blue). Note that the Atlantic Ocean heat transport (Fig. 4a) and the global atmospheric heat transport (Fig. 5) are mostly opposite in direction to each other. Prior to the weakest SAMHT (i.e., 15-yr lag), the atmospheric heat transport is northward. There is anomalous positive HC over most of the South Atlantic (Fig. 4b) and negative HC north of 20°N, supporting the northward atmospheric heat transport. This positive meridional gradient in oceanic HC is consistent with the anomalous Hadley circulation about 15–20 years after the negative SAMHT anomaly (Fig. 5, green line), which transports atmospheric heat southward. Therefore, the SAMHT leads the atmospheric heat transport response by about 15–20 years.

In summary, on decadal time scales, the interhemispheric global atmospheric mass and heat transports are directly linked to the HC of the tropical Atlantic Ocean, which is modulated by the SAMHT. The maximum northward atmospheric transport, which occurs about 15–20 years before the peak SAMHT, is forced by the interhemispheric gradient of Atlantic Ocean heat content (Fig. 4b). The maximum southward atmospheric transport at 0-yr lag is mostly due to the anomalous positive North Atlantic Ocean heat content (maximum at about 15°N) formed by heat transport convergence 15–20 years earlier. Of key importance is what occurs after the minimum in SAMHT (i.e., after 0-yr lag). The maximum southward atmospheric transport at about 15–20-yr lead (Fig. 5) is forced by a dipole in the Atlantic Ocean heat content, induced mostly by heat transport divergence over the South Atlantic at 0-yr lag. This result suggests that SAMHT could provide lead-time predictability of the state of the zonal mean atmospheric circulation. For this, the next section will focus on the atmospheric response to the SAMHT anomaly delayed by 20 years.

4. Atmospheric response to SAMHT variability at 20-yr lead time

Before assessing decadal changes in the global atmospheric response as a function of the SAMHT, we first discuss the global distribution of heat budget for the atmosphere and ocean at 20-yr lead time after the anomalous SAMHT. For this, we use monthly mean radiative fluxes at the top of the atmosphere (TOA) consisting of net incoming solar radiation and net outgoing radiation. There is large interhemispheric asymmetry in the distribution of radiative fluxes at TOA, with the NH receiving a net flux of 0.14 PW and the SH losing 0.26 PW. There should be a net southward heat transport by the combined ocean and atmosphere system, which is shown by the hemispheric asymmetry of upper-ocean heat content in Fig. 4b. Overall, there is an interhemispheric difference of about 0.4 PW in both the ocean and atmosphere at 20-yr lead time after the anomalous negative SAMHT. This is roughly the same amplitude as the decadal variability of SAMHT. This asymmetry must be balanced by meridional heat transport. The composite difference of 500-mb temperature (1 mb = 1 hPa), SST, and precipitation is shown in Fig. 6 at 20-yr lead time. There is tropospheric cooling

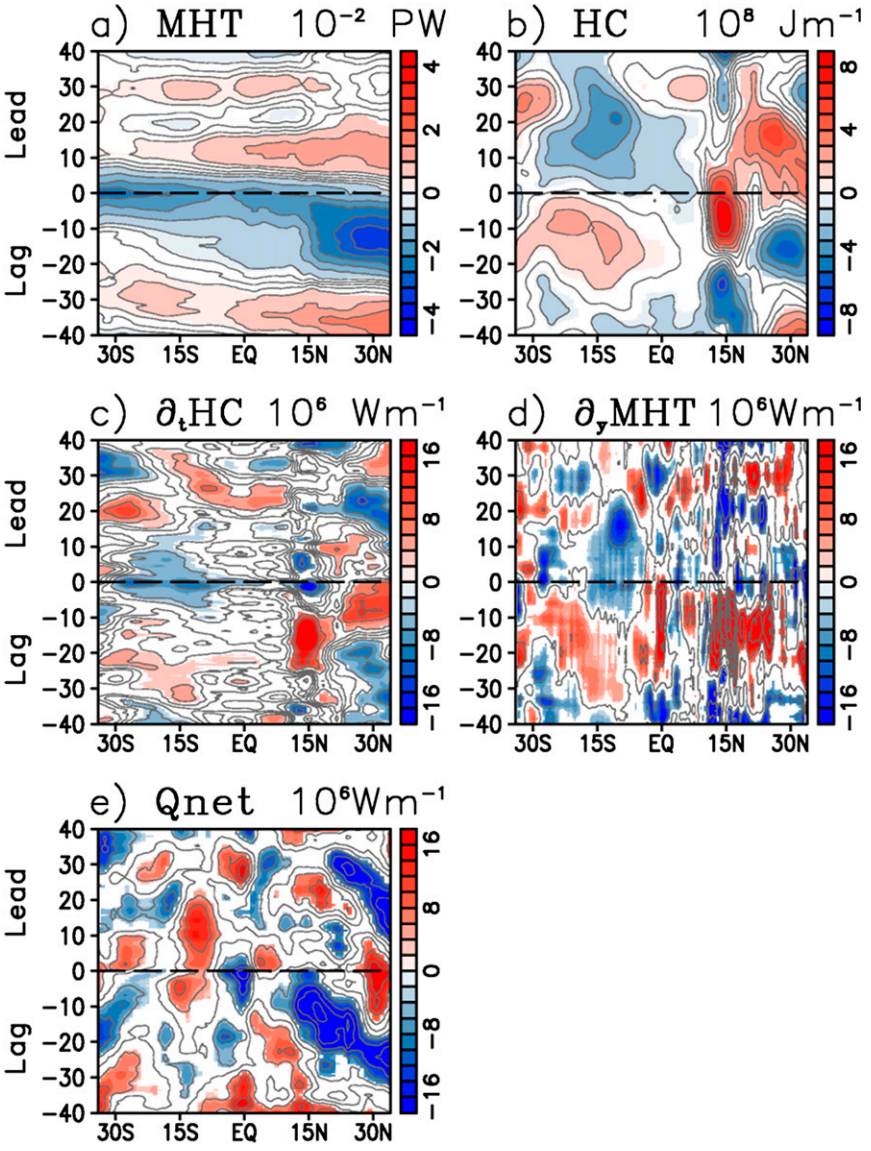

FIG. 4. (a) Lead–lag composite difference of zonal mean Atlantic MHT with respect to weak minus strong SAMHT. (b)–(e) As in (a), but for 700-m Atlantic Ocean HC, heat content tendency, MHT divergence (positive for convergence), and net surface energy flux (positive downward into the ocean), respectively. Color shading indicates 95% significance using a Student's *t* test. The *y* axis indicates time in years. Time progresses up the panels with lag (lead) indicating SAMHT lags (leads), respectively.

(warming) in the SH (NH) associated with SST anomalies of the same sign. The largest SST anomaly occurs over the South Atlantic, consistent with the negative heat content there, as shown in Fig. 4b. Although the SST forcing is zonally asymmetric, atmospheric eddies and westerlies homogenize it into a symmetric atmospheric response (Kang et al. 2014). This creates an equatorially asymmetric precipitation response in the tropics (Fig. 6c), with positive (negative) anomaly in the NH (SH). A study by Sun et al. (2013) investigated the relationship between the equatorially asymmetric precipitation and interhemispheric SST dipole. They found that this SST dipole arises from variability related to northward cross-equatorial ocean heat transport, with potential influence on decadal variability of tropical precipitation. The role of atmospheric eddies and the mean circulation is discussed next.

Atmospheric circulation associated with the SAMHT is assessed by analyzing the composite of the weak minus strong SAMHT, 20 years after the anomalous SAMHT. Here, a zonal mean approach is adopted to quantify the meridional fluxes of heat and moisture. Figure 7a shows the time mean and zonal mean meridional circulation (MMC) of the atmosphere as measured by the mass streamfunction (contour) and composite

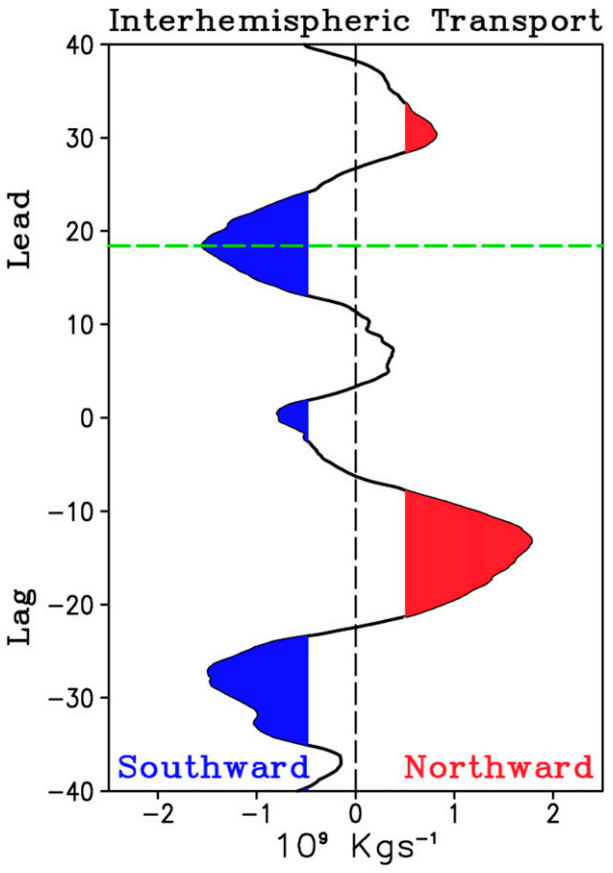

FIG. 5. Lead–lag composite difference of interhemispheric atmospheric circulation depicted as the vertically integrated mass transport about the equator for weak minus strong SAMHT. Here, the direction of interhemispheric atmospheric heat transport is proportional to the mass transport with northward (southward) labeled red (blue). Color shading indicates 95% significance using a Student's t test. The y axis indicates time in years. Time progresses up the panel with lag (lead) indicating that SAMHT lags (leads), respectively.

difference (color). Figures 7b and 7c are identical to Fig. 7a, but for the meridional heat flux and meridional moisture flux, respectively. Here, heat flux associated with MMC is defined as $[\overline{v}][\overline{T}]$, and moisture flux is $[\overline{v}][\overline{q}]$, where v is the meridional wind, T is the temperature, and q is the specific humidity. The overbar represents time mean and brackets represent zonal mean. Northward heat and moisture flux are indicated by positive contours. The Hadley circulation is a thermally direct circulation that transports heat by its upper branch (i.e., away from the equator) and moisture by its lower branch (i.e., toward the equator). The MMC (Fig. 7a) shows anomalous negative streamfunction around the equator of the order of 10% of the mean circulation. This is indicative of strengthening (weakening) of the SH (NH) Hadley circulation about 20 years after the weakening of the SAMHT. Implications for this circulation pattern are highlighted in Figs. 7b and 7c in that there are anomalous interhemispheric heat and moisture fluxes (NH-to-SH heat flux and SH-to-NH moisture flux). Similar to the MMC anomalies, the composite differences in the heat and moisture fluxes are also both about 10% of the mean fluxes and are located near the equator. This anomalous circulation pattern implies strengthening of the ITCZ to the north of the equator (e.g., 15°N) where moisture flux convergences at lower levels and heat flux divergence at upper levels increase the convective available potential energy (CAPE) and thus strengthen the NH summer monsoon via the so-called interhemispheric teleconnection mechanism (e.g., Lee et al. 2013).

The MMC is well known to be crucial in heat and moisture distribution from the equator to higher latitudes. However, atmospheric eddies, stationary and transient, are also important in heat distribution at midlatitudes. In a zonal mean state, stationary and transient eddy heat flux is toward the poles. These eddies result from the unstable equator-to-pole radiative–convective equilibrium temperature gradient. Besides the poleward heat transport, eddies are important in transporting angular momentum poleward, which maintains the easterly winds in the tropics and westerlies in midlatitudes. Similar to Fig. 7, Fig. 8a depicts the 500-mb mean transient eddy heat flux (black) and composite difference (green) corresponding to the weak minus strong SAMHT at 20-yr lead time. Transient eddy flux is defined as $[\overline{v'T'}]$—the product of meridional wind and temperature anomalies. The primes indicate anomalies, defined by the departure of the daily data from their monthly mean. Positive heat flux indicates northward flux. The anomalous heat flux is about 10% of the total heat flux. The total heat flux is stronger between 45° and 60° in both hemispheres. This is typically the location of the maximum momentum flux convergences, and hence the location of the maximum zonal wind. The anomalous heat flux (green line) is negative and equatorward (i.e., 30°) from the location of the strongest mean heat flux in both hemispheres. This suggests a poleward (equatorward) shift in the NH (SH) storm track or the mean location of the midlatitude transient eddies. As a consequence, the anomalous transient eddy heat flux works to cool (warm) the midlatitudes in the NH (SH), indicating heat flux divergence (convergence). That is, eddies work to reduce the anomalous temperature shown in Fig. 6a. Eddy heat flux convergence must be balanced by ascending motion (red region in Fig. 8a). Similarly, eddy heat flux divergence must be balanced by subsidence motion (blue region in Fig. 8a).

The zonal mean stationary eddy heat flux and composite difference are shown in Fig. 8b. Stationary eddy

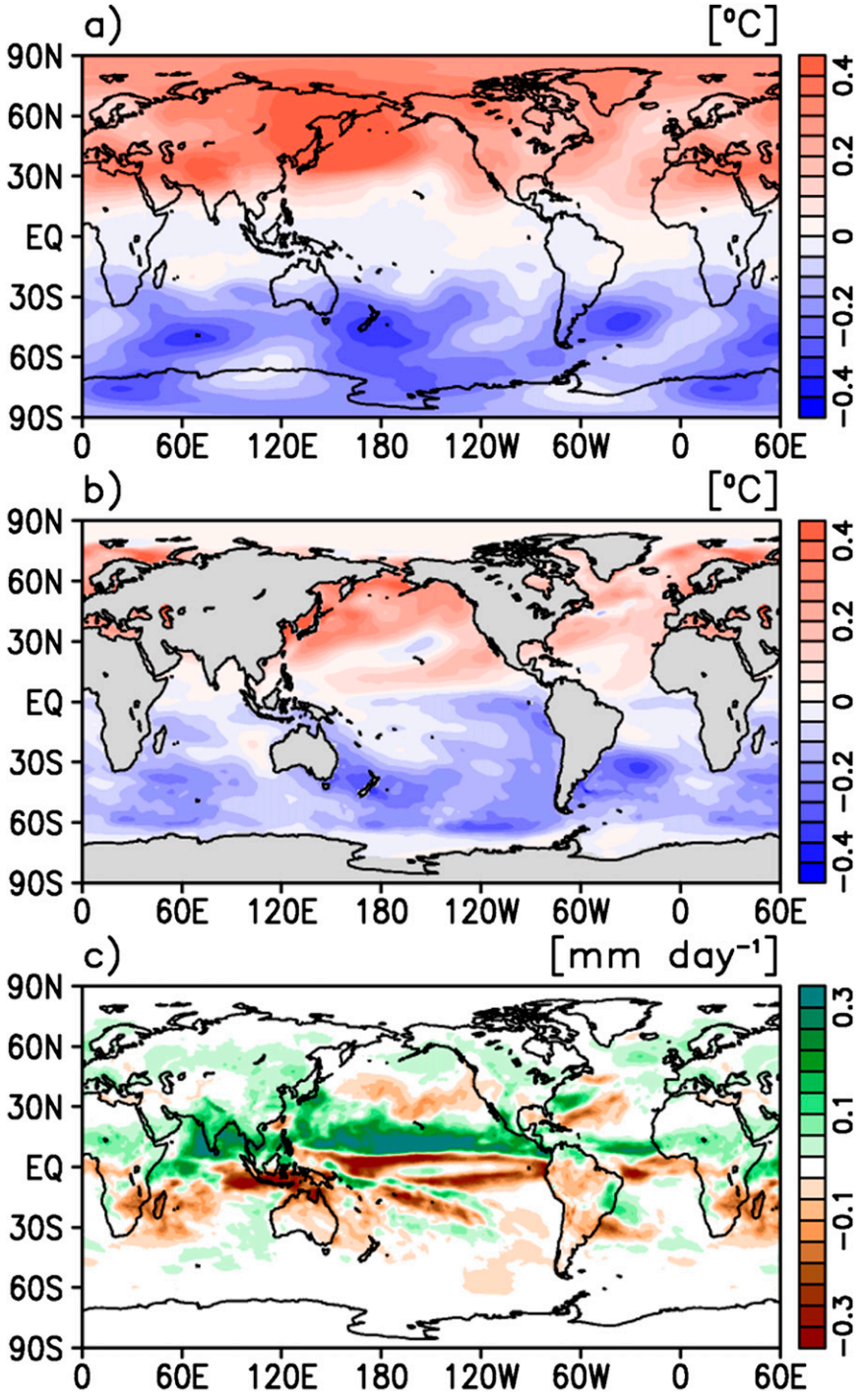

FIG. 6. Composite difference of (a) 500-mb air temperature, (b) sea surface temperature, and (c) precipitation corresponding to weak minus strong SAMHT at 20-yr lead time (i.e., 20 yr after the anomalous SAMHT).

fluxes are defined as $[\overline{v^*T^*}]$, where the stars indicate deviation from zonal mean. The strongest heat flux occurs at upper levels and near the surface. The anomalous heat flux is also on the order of 10% of the mean flux. Similar to the transient eddies, the anomalous heat flux is in the same (opposite) direction to that of the mean stationary eddy flux in the SH (NH). This suggests that stationary eddies are strengthened

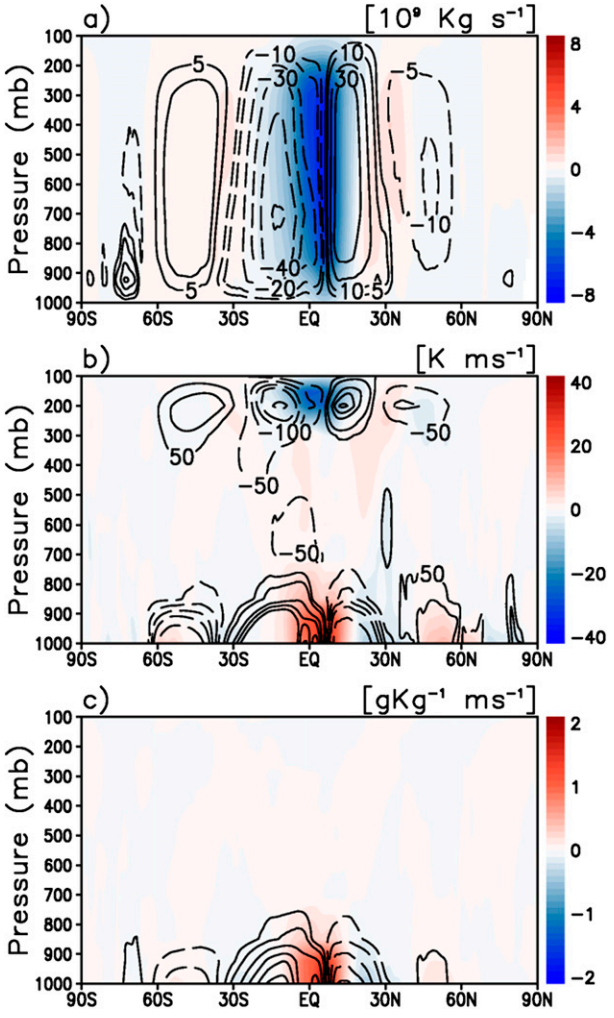

FIG. 7. (a) Time mean and zonal MMC of the atmosphere as measured by the mass streamfunction (contour) and composite difference (color) with respect to weak minus strong SAMHT at 20-yr lead time (i.e., 20 yr after the anomalous SAMHT; see Fig. 4). (b),(c) As in (a), but for the meridional heat flux and meridional moisture flux, respectively. Mean northward heat and moisture flux are indicated by positive contours and positive shading depicts anomalous northward fluxes.

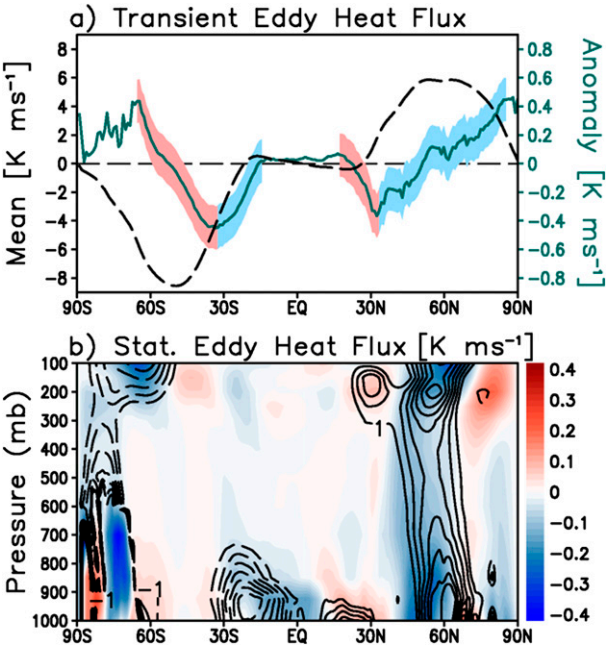

FIG. 8. (a) The 500-mb mean transient eddy heat flux (black dashed) and composite difference (green) during weak minus strong SAMHT. Anomalous heat flux convergence (divergence) is highlighted by red (blue) regions on the composite difference line. (b) Stationary eddy heat flux (black contour) and composite difference (color shading) during weak minus strong SAMHT. As in Fig. 7, but the composite difference is analyzed 20 yr after the anomalous SAMHT.

in the SH and weakened in the NH when the SAMHT is weaker.

Over the midlatitudes, eddy heat flux convergence (divergence) is primarily balanced by ascending (descending) motion. Similarly, momentum flux convergence (divergence) is balanced by westerly (easterly) acceleration. It was shown that 20 years after the weak SAMHT, heat fluxes from transient and stationary eddies converge (diverge) over the subtropical NH (SH). This indicates that atmospheric eddies work in the same direction as the anomalous MMC (Fig. 7a) to produce anomalous ascending (descending) motion over the NH (SH) tropics, enhancing the north-to-south interhemispheric heat flux. The anomalous eddy heat flux poleward of 30°N (30°S) diverges (converges), producing subsidence (ascent) in the NH (SH). A more detailed discussion on the SAMHT role in modifying interhemispheric atmospheric transports will be presented in the discussion section.

5. Modulation of the NH summer monsoons

Results presented in earlier sections show that multidecadal variation in SAMHT plays a key role in the global redistribution of heat and freshwater. It was also shown that it could provide about 15–20-yr lead time information on the atmospheric transport, including anomalous interhemispheric Hadley circulation. An important question that remains is whether such anomalous atmospheric heat and moisture transport modulates monsoonal circulation, and whether the SAMHT could be used as a potential predictor of decadal variability of the monsoons. To address this question, we will focus our attention on the NH summer monsoon season. A motivation for this question is that the NH summer climate is strongly influenced by tropical convection associated with the convectively active monsoon phase.

The monsoon is a robust component of seasonal variability. Its occurrence is highly dependent on the seasonal cycle of solar radiation, which gives rise to land–sea temperature contrast (e.g., Li and Yanai 1996; Webster et al. 1998). Beyond seasonal variations, interannual variation of the monsoon is strongly influenced by larger-scale SST anomalies linked to El Niño–Southern Oscillation (ENSO; Wang et al. 2013). Therefore, monsoon simulations require the use of coupled models that capture interaction among all climate components. Ocean–atmosphere coupling may also introduce large errors due to uncertainties in the air–sea fluxes (Bollasina and Nigam 2009), in that small errors in one component of the climate system can be exacerbated by the other components. Sperber et al. (2013) analyzed the boreal summer Asian monsoon in models from phases 5 and 3 of the Coupled Model Intercomparison Project (CMIP5 and CMIP3). They found an improvement in the simulation of monsoon circulation and precipitation from CMIP3 to CMIP5 models, where the later models can reproduce some aspects (e.g., time mean, annual cycle, intraseasonal, and interannual variability) of the monsoon.

Here, we will use precipitation and 850-mb wind to characterize monsoon circulation in CESM1. The seasonality of global precipitation is well represented by CESM1 compared to the GPCC precipitation product (not shown). The largest seasonal range of precipitation is concentrated on a narrow equatorial band mostly over land (e.g., southern Asia, West Africa, and Central America in the Northern Hemisphere and the Amazon basin, southeastern Africa, and the Maritime Continent in the SH). Here, monsoon regions are identified by where the June–September (JJAS) minus December–March (DJFM) annual precipitation range is greater than $2\,\mathrm{mm\,day^{-1}}$ and the local summer precipitation exceeds 55% of the total annual precipitation, following Wang et al. (2012). There are five monsoonal circulations in the NH. They are the Indian (INDM), East Asian (EAM), western Pacific (WPNM), North American (NAM), and North African (NAF) monsoons. The INDM, EAM, and WPNM are often studied as one monsoon circulation, referred to as the Asian summer monsoon (Webster and Yang 1992). However, other studies have argued that the INDM and the EAM–WPNM systems owe to two distinct convective heat sources (Goswami et al. 1999; Wang and Fan 1999), where the former is forced by convection over the Arabian Sea and Bay of Bengal and the latter by convection over the South China Sea and the Philippines Sea, and that these two convective systems are poorly correlated. Consequently, this calls for the use of separate indices to study these monsoons.

Before analyzing the relationship between SAMHT and the monsoons, it is necessary to assess whether the model used here correctly simulates observed features of precipitation in the monsoon regions. CESM1 model reproduces the mean seasonal cycle for all monsoon regions, although with considerably weaker precipitation during the active phase (Fig. 9, left). Precipitation associated with the EAM is significantly weaker throughout the year when compared to the observed. The NAM and NAF monsoons are better represented in the model compared to the other monsoons.

The lag–lead relationship of SAMHT and NH monsoons is investigated here motivated by the zonally symmetric precipitation response in the tropics (Fig. 6c). Here, Spearman rank correlation is chosen over Pearson correlation as the former is a nonparametric test that does not make assumptions on the distribution of the data. It also does not make an assumption of linear relationships between each variable. These two assumptions are especially troublesome for the analysis of precipitation over monsoon regions where precipitation could be non-normally distributed and its relationship with other climate indices (e.g., SAMHT) could be nonlinear. To test the statistical significance of Spearman rank correlation, we rely on a nonparametric test known as the Kendall τ test that measures the degree of dependence between two variables by comparing the number of concordant versus the number of discordant pairs.

Figure 9 (right panels) shows the lag–lead Spearman ranked correlation between SAMHT and the NH monsoon index. The blue dashed lines depict the 95% significance level based on a nonparametric Kendall τ test. Negative lag indicates periods when SAMHT leads the NH monsoon index. Note that the SAMHT and NH monsoon indices are significantly anti-correlated when the SAMHT leads by 15–20 years. This is consistent with result described earlier in that the atmospheric response is preceded by SAMHT by 15–20 years. This negative correlation is indicative of a strengthening of the NH monsoon precipitation when SAMHT is weak. It also suggests that SAMHT could serve as a potential predictor for decadal variability of tropical NH precipitation.

Figures 10a,c,e,g show the seasonality of precipitation and 850-mb winds for the INDM, EAM, NAM, and NAF monsoon regions as measured by the difference in JJAS minus annual mean precipitation and winds. Multidecadal variability of monsoonal circulation and precipitation is analyzed as before by the composite difference corresponding to weak minus strong SAMHT at 20-yr lead time after the anomalous SAMHT. Figures 10b,d,f,h depict the composite difference of JJAS precipitation (shaded) and 850-mb rotational wind component for each monsoon region. Blue stippling indicate regions where precipitation

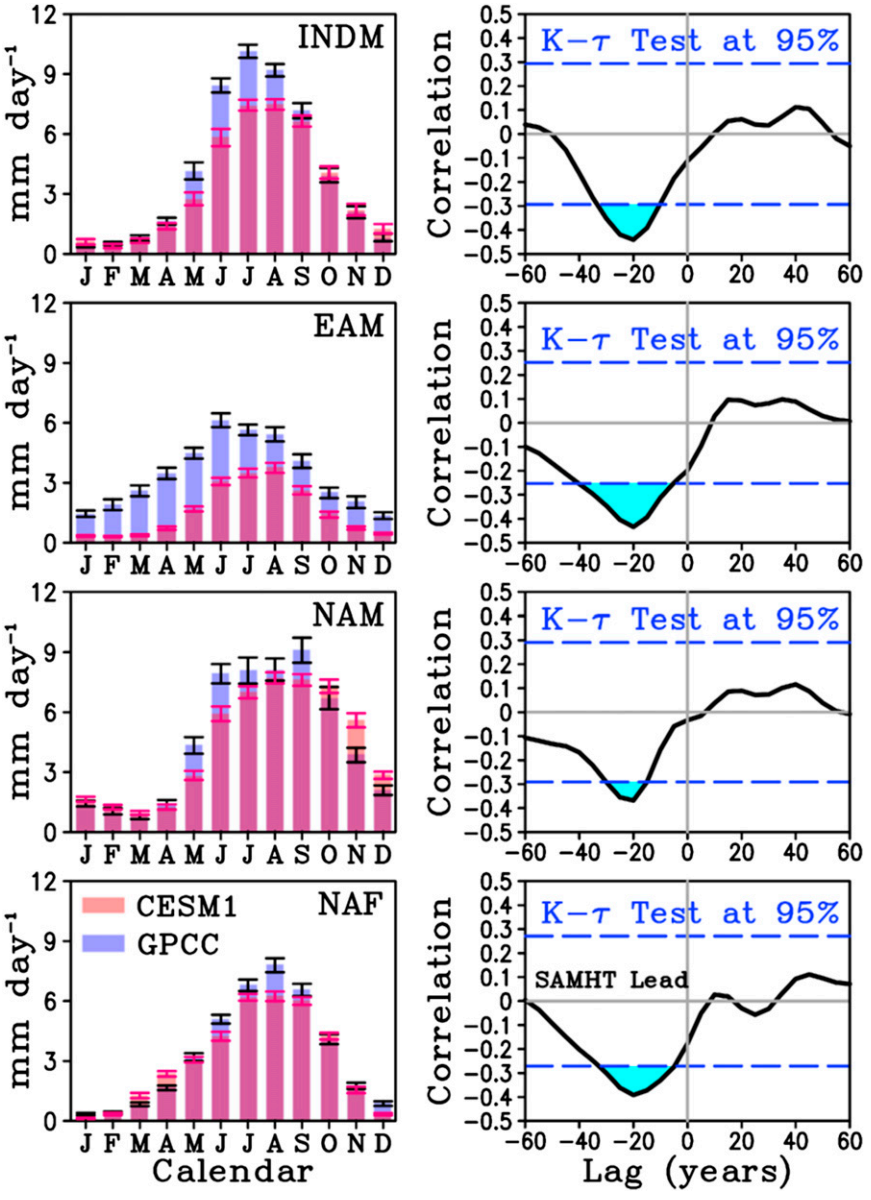

FIG. 9. (left) Seasonality of precipitation of the four monsoon regions [i.e., (top)–(bottom) INDM, EAM, NAM, and NAF] from GPCC (blue) and CESM1 (red). Error bars indicate the 99% confidence level. (right) Lag–lead Spearman ranked correlation between SAMHT and NH monsoon index. The blue dashed lines depict the 95% significance level based on a nonparametric Kendall τ test. Negative lag indicates periods when SAMHT leads the NH monsoon index. Periods with significant correlation are shaded blue.

differences are significant at 95% confidence level based on a nonparametric Kolmogorov–Smirnov test. This nonparametric test measures whether two samples (e.g., weak SAMHT period and strong SAMHT periods) have different distribution. Each region is discussed separately below.

1) The INDM (Findlater 1969; Yim et al. 2014) circulation is associated with low-level southwesterlies and precipitation anomaly from the Arabian Sea to the Bay of Bengal (Fig. 10a). Multidecadal variability associated with weaker SAMHT is identified by enhanced precipitation over the Indian subcontinent and the Arabian Sea and less precipitation over the Indian Ocean (Fig. 10b). The circulation pattern shows an enhanced southwesterly low-level jet associated with cyclonic circulation, which brings moisture convergence over India. This pattern reinforces the low-level southwesterly flow associated with the summer INDM.

2) The EAM (Yim et al. 2014) is a unique monsoon due to its higher-latitude location. It presents itself as a dipole in precipitation (Fig. 10c). The composite difference shows a clear dipole in precipitation with positive (negative) anomaly over eastern China (East China Sea). Low-level anticyclonic circulation centered over southern Japan favors southwesterly flow toward eastern China and the Korea Peninsula, bringing moisture from the Pacific Ocean. The decadal variability associated with SAMHT presents a northward shift and intensification of this monsoon with respect to climatology.
3) Although the NAM is not as robust as the other monsoons mentioned above, it is an important component in seasonal precipitation over northwestern Mexico and the southwestern United States (Adams and Comrie 1997; Barlow et al. 1998; Cook and Seager 2013), accounting for over 70% of the annual total rainfall in these regions. The composite difference shows enhanced precipitation over western Mexico and the tropical eastern North Pacific Ocean (Fig. 10f). This is associated with moisture flux convergence over this region and consistent with strengthening of the summer monsoon (Fig. 10f).
4) For the NAF (Yim et al. 2014), the composite difference shows enhanced precipitation and a low-level westerly jet, bringing moisture from the Atlantic Ocean toward the Sahel region (Fig. 10h). This is consistent with the intensification of the westerlies and cross-equatorial flow from the Atlantic Ocean observed during the summer NAF monsoon (Fig. 10g).

In summary, all NH summer monsoons are enhanced during weaker a SAMHT. This is consistent with enhanced moisture transport from the Southern to the Northern Hemisphere by the anomalous Hadley circulation. Recall that there is weaker zonal flow due to anomalous southward eddy heat flux over the NH north of 25°N. This creates eddy heat flux convergence and ascending motion, thereby enhancing precipitation over these monsoon regions. These are important results suggesting that the SAMHT is a potential source of predictability, with about 20-yr lead time, of NH summer monsoon variability.

6. Relative influence of the North and South Atlantic on atmospheric circulation

Our analysis in previous sections indicates that decadal variability of SAMHT could modulate global atmospheric circulation and monsoons. However, since a similar link between NAMHT and global monsoons could potentially exists, it is important to understand the relative roles of SAMHT and NAMHT in modulating global monsoon variability. In other words, we need to identify whether SAMHT offers decadal predictability of global monsoons independent from that of NAMHT, which is a much more widely used index of AMOC and associated heat transport. Figure 11 depicts the anomalous interhemispheric atmospheric mass transport corresponding to weak minus strong SAMHT (Fig. 11a) and weak minus strong NAMHT (Fig. 11b), similar to Fig. 5. Here, we are interested in those periods where the NAMHT and SAMHT lead the atmospheric transport (i.e., positive leads). There exists southward (i.e., negative) anomalous atmospheric heat transport about 18 years after the negative SAMHT anomaly (Fig. 11a, green line). This is also observed in the case of NAMHT, but for lead time of about 25 years (Fig. 11b, green line).

There is a difference in atmospheric response lead times between NAMHT and SAMHT, which is depicted by diagonal magenta line between Figs. 11a and 11b; however, this does not mean that SAMHT variability is independent of NAMHT. In fact, SAMHT variability is preceded by NAMHT variability, suggesting that the North Atlantic could provide more lead time predictability than SAMHT. To further test, we attempted to separate the influence of the SAMHT and NAMHT on atmospheric transport by using conditional composite analysis and partial regression analysis. For this manuscript, we opt to show results from conditional composite analysis to be consistent with the rest of the paper, although both analyses give consistent results.

Figure 11c shows the annual mean (thin black) and composite difference of atmospheric MMC as measured by the zonal mean 500-mb atmospheric mass streamfunction. The composite difference is centered at lead times according to that of Figs. 11a and 11b (dashed green lines). The conditional composite for MMC (i.e., dependent variable) is built based on the state of the SAMHT and NAMHT (i.e., independent variables). Positive (negative) values indicate northward (southward) mass transport. Note that the influence of a weakening of SAMHT and NAMHT onto the MMC has similar amplitude. Also, the amplitude of the MMC anomaly is larger when both MHT indices are considered. This suggests that both the SAMHT and NAMHT and associated HC anomalies influence atmospheric circulation and transport. However, the NAMHT leads the SAMHT negative HC anomaly in the South Atlantic associated with SAMHT divergence works in par with positive HC anomaly in the North Atlantic due to NAMHT convergence (see Fig. 4b), creating an interhemispheric asymmetry in energy balance. This asymmetry drives an anomalous Hadley circulation which transport heat from the NH to the SH (Fig. 11c, green contour).

Several studies have suggested that the NAO is a precursor of NAMHT variability, through wind stress

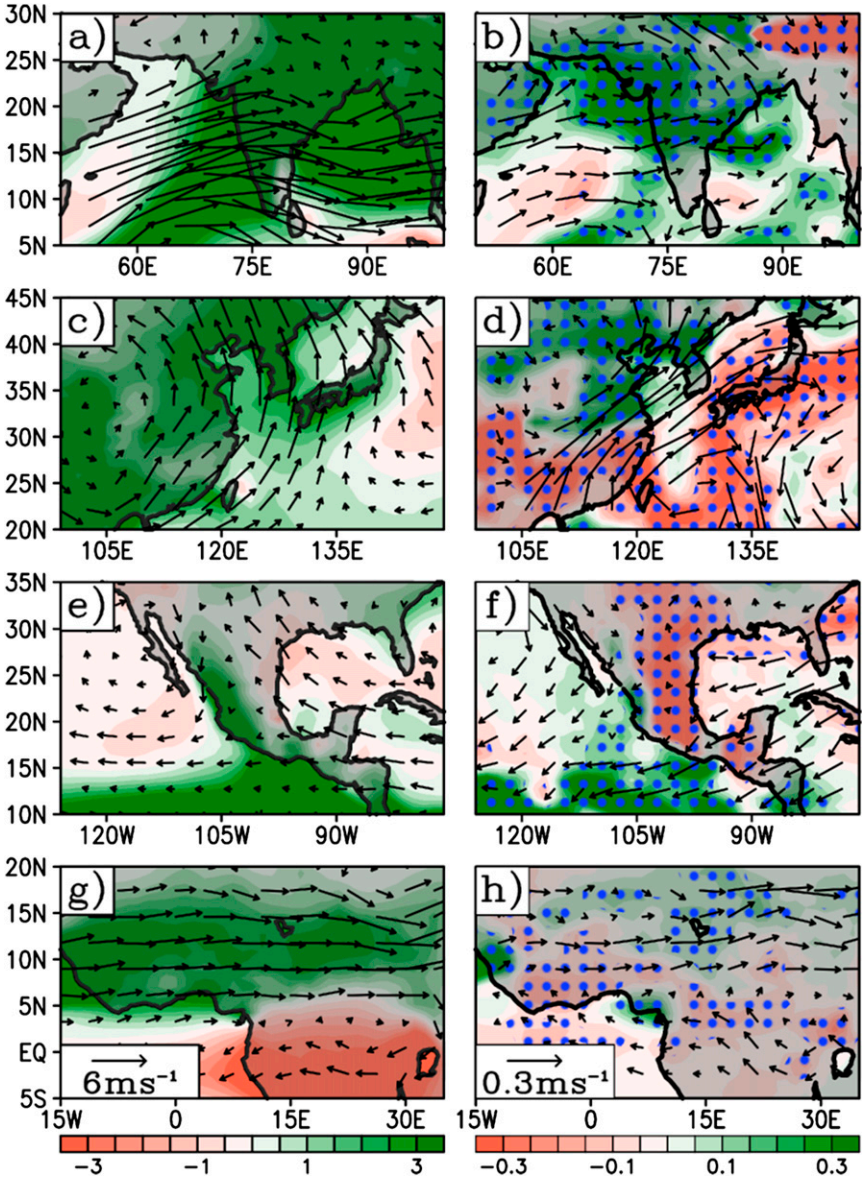

FIG. 10. (a),(c),(e),(g) Seasonality of precipitation and 850-mb winds for the monsoon regions INDM, EAM, NAM, and NAF, respectively, as measured by the difference between JJAS minus annual mean precipitation and winds. (b),(d),(f),(h) The composite difference of JJAS precipitation (shaded) and 850-mb wind for each monsoon region with respect to weak minus strong SAMHT at lead time of 20 yr after the anomalous SAMHT. Blue stippling indicates regions where precipitation differences are significant at 95% confidence level based on a nonparametric Kolmogorov–Smirnov test.

and heat flux forcing in the high-latitude oceanic convection regions (e.g., Eden and Willebrand 2001; Medhaug et al. 2012; Sun et al. 2015b). Here, we address the relationship of NAMHT and SAMHT with the NAO. Figure 12a shows the lag–lead composite difference of NAO index for weak minus strong SAMHT (red) and NAMHT (blue). As suggested in Sun et al. (2015b), the negative phase of the NAO precedes the weakening of NAMHT by about 15 years. This delayed effect is due to large inertia associated with slow oceanic processes. The reduced AMOC and NAMHT have a negative feedback in that the NAO shows a delayed response (i.e., positive phase) about 18 years after the weakening of the NAMHT. However, the relationship between SAMHT and NAO is not robust. Thus, NAO does not give a predictability of SAMHT.

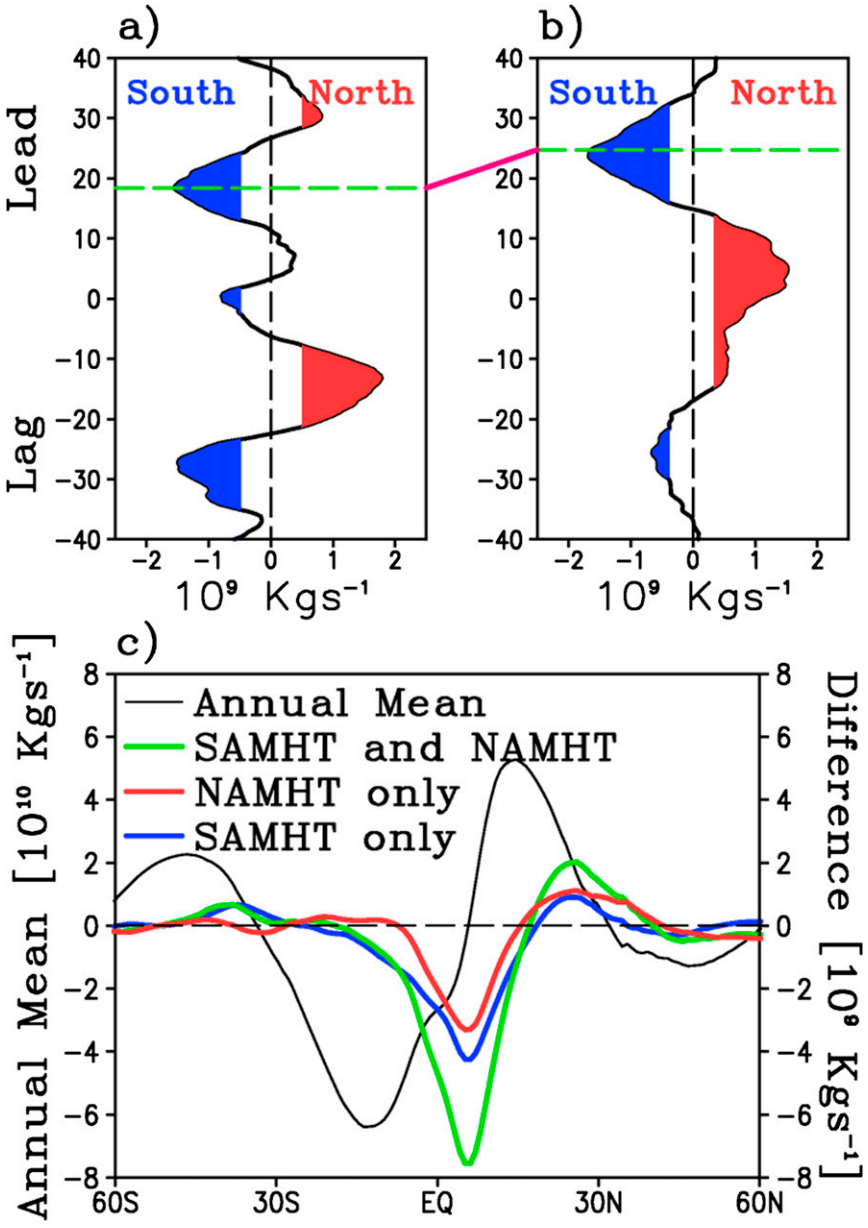

FIG. 11. Anomalous interhemispheric atmospheric mass transport corresponding to (a) weak minus strong SAMHT and (b) weak minus strong NAMHT, as in Fig. 5. The diagonal magenta line between (a) and (b) highlights the fact that NAMHT leads SAMHT. (c) Annual mean (thin black) and composite difference of atmospheric MMC as measured by the zonal mean 500-mb atmospheric mass streamfunction. The composite difference is centered at lead times according to that of (a) and (b) (dashed green lines). The conditional composite for MMC (i.e., dependent variable) is built based on the state of the SAMHT and NAMHT (i.e., independent variables). The green contour here includes the relationship between the MMC with both SAMHT and NAMHT. The red contour depicts the relationship between NAMHT and the MMC excluding the influence of SAMHT (i.e., neutral SAMHT periods based on terciles). Similarly, the blue contour shows the relationship between SAMHT and the MMC excluding the influence of NAMHT (i.e., neutral NAMHT periods based on terciles). Positive (negative) values indicate northward (southward) mass transport.

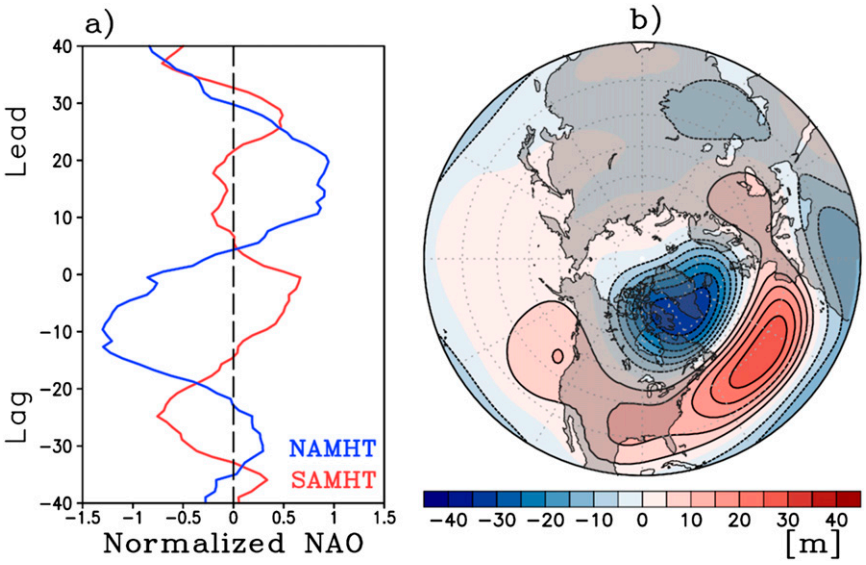

FIG. 12. (a) Lead–lag composite difference of the NAO index for weak minus strong SAMHT (red) and weak minus strong NAMHT (blue). The *y* axis indicates time in years. Time progresses up the panel with lag (lead) indicating the ocean MHT lags (leads), respectively. (b) The 500-mb geopotential height anomaly associated with the positive phase of the NAO.

7. Summary and discussion

This study tested the hypothesis whether low-frequency (decadal) variability of the South Atlantic meridional overturning circulation and MHT influence decadal variability of climate events over the globe. A multicentury climate simulation based on a state-of-the-art coupled GCM was used as the basis for our analysis. Multidecadal variability of the South Atlantic Ocean has been shown to play a key role in modulating atmospheric dynamics including the distribution of momentum, heat, and freshwater. For this reason, it is of great importance to the climate community to understand the role that the ocean plays and the physical mechanism behind this hypothesis. In this section, we highlight this mechanism, which was described in previous sections, using two summary schematic diagrams presented in Figs. 13 and 14.

The first diagram (Fig. 13) shows the transient evolution of MHT anomaly over the tropical Atlantic Ocean during weak minus strong SAMHT. Here, the gray shading indicates the anomalous negative MHT (i.e., weakening of the northward heat transport). The anomaly propagates from north to south (black arrows), where the anomaly at 30°N leads the anomaly at 30°S by about 10–12 years with a speed of approximately 600 km yr^{-1}. The largest amplitudes occur away from the equator. When the maximum anomaly arrives at 30°S (i.e., the location of our composite SAMHT or 0-yr lag), there is MHT divergence between 30°S and the equator, highlighted by the dark-blue hatching and easily identified by the increased MHT southward away from the equator. The MHT divergence is balanced by negative heat content tendency, which results in negative heat content anomaly over the South Atlantic and negative SST anomaly about 15–20 years later, shown by blue shading. The positive heat content anomaly in the NH is mostly due to MHT convergence approximately 10–12 years earlier. This creates an interhemispheric HC anomaly. The impact of these heat content anomalies on atmospheric circulation is discussed next.

The diagram in Fig. 14 shows the zonal mean atmospheric (top) and Atlantic Ocean (bottom) circulation. As discussed with respect to Fig. 13, weaker MHT (thick arrows at the bottom of the panel) is associated with negative tendency in heat content over the subtropical South Atlantic (blue stippling at 0-yr lag in Fig. 13). The heat content tendency is dominated by meridional MHT divergence (blue stippling in Fig. 13), producing a negative heat content anomaly approximately 15–20 years later. The negative (positive) heat content anomaly in the SH (NH) forces subsidence and anomalous Hadley circulation (gray oval and counterclockwise circulation in Fig. 14) that brings moisture from the SH to the NH (green arrow) and heat from the NH toward the SH (purple arrow). This anomalous interhemispheric atmospheric circulation is supported by a net gain in radiative fluxes at the top of the atmosphere (labeled R_{TOA}) over the NH and net radiative loss over the SH represented by red and blue arrows, respectively. In

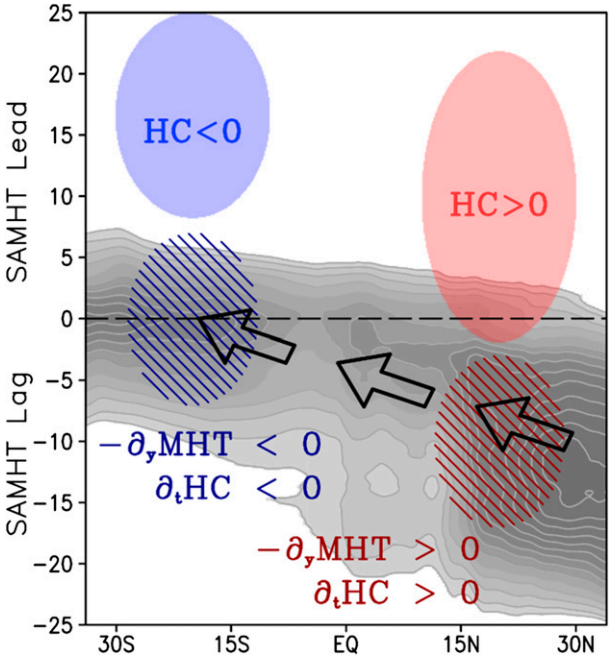

FIG. 13. Transient evolution of MHT anomaly over the tropical Atlantic Ocean during weak minus strong SAMHT. Gray shading indicates the anomalous negative MHT (i.e., weakening of the northward heat transport). The anomaly propagates from north to south (black arrows) at about 600 km yr^{-1}. The dark-red hatched region indicates MHT convergence and positive heat content tendency north of the equator 10–15 yr prior to the weak minus strong SAMHT, whereas the dark-blue hatched region indicates MHT divergence and negative heat content tendency south of the equator near 0-yr lag with respect to weak minus strong SAMHT. Blue (red) shading depicts negative (positive) heat content. The *y* axis indicates time in years. Time progresses up the panel, with lag (lead) indicating SAMHT lags (leads), respectively. Anomalous heat content occurs about 15–20 yr after the anomalous heat content tendency and heat transport divergence in both hemispheres.

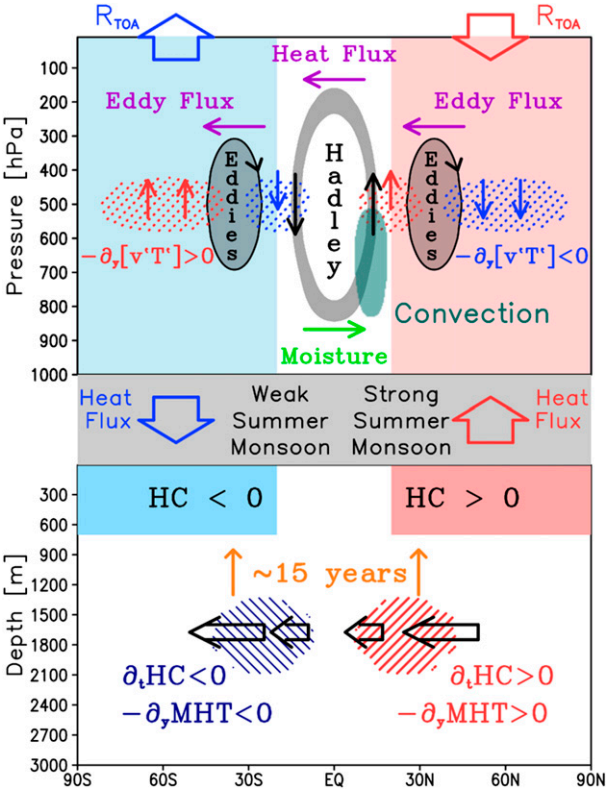

FIG. 14. Schematic diagram of the role of weaker-than-normal MHT in the anomalous atmospheric circulation at 15–20-yr lead time. Weakened MHT is shown by thick black arrows at the bottom of the panel. Negative (positive) tendency in heat content is labeled by dark blue (red) hatching. There is negative (positive) heat content in the SH (NH) about 15–20 yr after the heat transport anomaly labeled here by blue (red) rectangle. Anomalous Hadley circulation is labeled by gray oval and counterclockwise circulation. Moisture and heat fluxes are shown by green and purple arrows, respectively. The TOA and surface radiative fluxes are shown by thick red and blue arrows. Purple arrows depict atmospheric eddy heat transports. Eddy forced vertical motion is shown by red and blue stippling. See discussion in main text for more detail.

addition, there is a net positive surface heat flux downward in the SH (blue arrows labeled heat flux). Atmospheric eddies, both transient and stationary, transport heat southward in both hemispheres (purple arrows) to balance the radiative fluxes. This produces eddy heat flux convergence around 15°N and divergence around 15°S (stippling), reinforcing the anomalous Hadley circulation. Poleward of 30° latitude, anomalous atmospheric eddies produce heat flux divergence (convergence) in the NH (SH), which causes sinking (rising) motion. This is consistent with a poleward (equatorward) displacement of the jet stream and mean storm track and enhanced (reduced) TOA radiation in the NH (SH). The poleward (equatorward) displacement of the jet stream is a consequence of thermal wind balance from a reduced (enhanced) meridional temperature gradient over NH (SH) midlatitudes. The poleward (equatorward) shift of the mean zonal jet in the NH (SH) causes eddy momentum flux convergence (divergence). This must be balanced by poleward (equatorward) flow at upper levels. This flow pattern supports a thermally indirect eddy-driven circulation in both hemispheres (circulation labeled eddies in Fig. 14). This circulation brings anomalous ascent and more precipitation from 15° to 30°N, and descent and less precipitation poleward of 30°N. The opposite occurs in the SH, with descent and less precipitation from 30° to 15°S and ascent poleward of 30°S. In summary, the NH atmosphere behaves like the summer hemisphere and conversely the SH behaves like the winter hemisphere, approximately 15–20 years after the anomalous negative SAMHT.

The proposed mechanism is in contrast to that of Sun et al. (2015a), which suggests that the North Atlantic MOC

can influence the SH midlatitude zonal wind and precipitation. They found that strengthening of the North Atlantic MOC induces a subpolar interhemispheric SST seesaw pattern, with cold SST anomalies in the high-latitude Southern Ocean. This leads to an enhanced meridional temperature gradient, increasing the zonal winds. The associated changes in the zonal wind could potentially influence SAMHT, explaining the lead–lag relationship of NAMHT and SAMHT. However, we found that the geostrophic component of the SAMHT explains most of the low-frequency variance of the total SAMHT, whereas the Ekman (i.e., wind-forced) component comprises higher frequencies. Further investigations on the contrasting mechanisms are necessary but beyond the scope of this study.

8. Conclusions

This is the first attempt to link the South Atlantic overturning circulation variability to weather and climate. The anomalous circulation pattern associated with SAMHT variability discussed throughout this paper has great implications for long-term climate variability over the whole globe. For example, it could bring drier and warmer summer conditions over North America and Europe. The results presented here suggest the possibility of decadal predictability of seasonal temperature and precipitation, more so for those regions affected by monsoonal circulation. It was shown that decadal modulation of the NH summer monsoon is tied to variability of the SAMHT. Intensification of the NH summer monsoon is through a northward shift and strengthening of the ITCZ when the SAMHT is weak via upper ocean heat content modification. This proposed mechanism utilizing the atmospheric energy budget to understand the ITCZ location is consistent with Kang et al. (2009) and Broccoli et al. (2006). Our hypothesis of a tropical control of the location of the ITCZ is in contrast with the possibility of a high-latitude control of the ITCZ location proposed in Frierson et al. (2013). The ITCZ in this study is shifted toward the warmer hemisphere, which is the NH, about 15–20 years after a weakening of the SAMHT.

The main objective here was to highlight the important role of the SAMHT in modifying atmospheric circulation. Most of the current literature focuses on the North Atlantic. Here, we showed that the South Atlantic variability offers potential for added predictability of the climate system. Our argument that the SAMHT could modify the strength and location of the ITCZ has important implications, because the slowly varying South Atlantic circulation could serve as potential predictor for decadal variability of the global monsoon system giving a lead time of about 15–20 years from the anomalous MHT to its climate effects. Since this is one of the first studies to investigate the role of the South Atlantic on climate and monsoons, further efforts are necessary to confirm these results. For example, the processes that are responsible for the SAMHT variability are unclear. Is the SAMHT only a consequence of North Atlantic variability, or is it driven by independent local processes in the South Atlantic such as those mentioned in the introduction? The relative roles of the North and South Atlantic MOC on the climate system need further investigation. In future work, special emphasis will be given to high-impact extreme weather events, such as droughts and heat waves. Also, the relative role of internal climate variability, like SAMHT, versus external forcing is an important question given the current climate projections (e.g., Lee et al. 2014). Results presented here highlight the need for continuous improvements in coupled models as well as the value of sustained ocean observational efforts, both of which are necessary to improve our knowledge of the complex interaction between the South Atlantic MOC and global climate variability.

Acknowledgments. We would like to acknowledge the three anonymous reviewers for their insightful comments. This research was carried out in part under the auspices of the Cooperative Institute of Marine and Atmospheric Studies, a cooperative institute of the University of Miami and the National Oceanic and Atmospheric Administration (NOAA), cooperative agreement NA10OAR4320143. This work was supported by NOAA/Atlantic Oceanographic and Meteorological Laboratory and funded by Climate Observations Division of the NOAA/Climate Program Office.

REFERENCES

Adams, D. K., and A. C. Comrie, 1997: The North American monsoon. *Bull. Amer. Meteor. Soc.*, **78**, 2197–2213, doi:10.1175/1520-0477(1997)078<2197:TNAM>2.0.CO;2.

Ambrizzi, T., B. J. Hoskins, and H.-H. Hsu, 1995: Rossby wave propagation and teleconnection patterns in the austral winter. *J. Atmos. Sci.*, **52**, 3661–3672, doi:10.1175/1520-0469(1995)052<3661:RWPATP>2.0.CO;2.

Barlow, M., S. Nigam, and E. H. Berbery, 1998: Evolution of the North American monsoon system. *J. Climate*, **11**, 2238–2257, doi:10.1175/1520-0442(1998)011<2238:EOTNAM>2.0.CO;2.

Becker, A., P. Finger, A. Meyer-Christoffer, B. Rudolf, K. Schamm, U. Schneider, and M. Ziese, 2013: A description of the global land-surface precipitation data products of the Global Precipitation Climatology Centre with sample applications including centennial (trend) analysis from 1901-present. *Earth Syst. Sci. Data*, **5**, 71–99, doi:10.5194/essd-5-71-2013.

Biastoch, A., C. W. Böning, F. U. Schwarzkopf, and J. Lutjeharms, 2009: Increase in Agulhas leakage due to poleward shift of Southern Hemisphere westerlies. *Nature*, **462**, 495–498, doi:10.1038/nature08519.

Bollasina, M., and S. Nigam, 2009: Indian Ocean SST, evaporation, and precipitation during the South Asian summer monsoon in IPCC-AR4 coupled simulations. *Climate Dyn.*, **33**, 1017–1032, doi:10.1007/s00382-008-0477-4.

Broccoli, A. J., K. A. Dahl, and R. J. Stouffer, 2006: Response of the ITCZ to Northern Hemisphere cooling. *Geophys. Res. Lett.*, **33**, L01702, doi:10.1029/2005GL024546.

Broecker, W. S., 1991: The great ocean conveyor. *Oceanography*, **4**, 79–89, doi:10.5670/oceanog.1991.07.

——, D. M. Peteet, and D. Rind, 1985: Does the ocean–atmosphere system have more than one stable mode of operation? *Nature*, **315**, 21–26, doi:10.1038/315021a0.

Cassou, C., C. Deser, L. Terray, J. W. Hurrell, and M. Drévillon, 2004: Summer sea surface temperature conditions in the North Atlantic and their impact upon the atmospheric circulation in early winter. *J. Climate*, **17**, 3349–3363, doi:10.1175/1520-0442(2004)017<3349:SSSTCI>2.0.CO;2.

——, L. Terray, and A. S. Phillips, 2005: Tropical Atlantic influence on European heat waves. *J. Climate*, **18**, 2805–2811, doi:10.1175/JCLI3506.1.

Cheng, W., J. C. H. Chiang, and D. Zhang, 2013: Atlantic meridional overturning circulation (AMOC) in CMIP5 models: RCP and historical simulations. *J. Climate*, **26**, 7187–7197, doi:10.1175/JCLI-D-12-00496.1.

Chiang, J. C., and C. M. Bitz, 2005: Influence of high latitude ice cover on the marine intertropical convergence zone. *Climate Dyn.*, **25**, 477–496, doi:10.1007/s00382-005-0040-5.

Clark, P. U., N. G. Pisias, T. F. Stocker, and A. J. Weaver, 2002: The role of the thermohaline circulation in abrupt climate change. *Nature*, **415**, 863–869, doi:10.1038/415863a.

Cook, B., and R. Seager, 2013: The response of the North American monsoon to increased greenhouse gas forcing. *J. Geophys. Res. Atmos.*, **118**, 1690–1699, doi:10.1002/jgrd.50111.

Corti, S., A. Weisheimer, T. Palmer, F. Doblas-Reyes, and L. Magnusson, 2012: Reliability of decadal predictions. *Geophys. Res. Lett.*, **39**, L21712, doi:10.1029/2012GL053354.

Cunningham, S. A., and Coauthors, 2007: Temporal variability of the Atlantic meridional overturning circulation at 26.5°N. *Science*, **317**, 935–938, doi:10.1126/science.1141304.

Danabasoglu, G., and J. Marshall, 2007: Effects of vertical variations of thickness diffusivity in an ocean general circulation model. *Ocean Modell.*, **18**, 122–141, doi:10.1016/j.ocemod.2007.03.006.

——, S. C. Bates, B. P. Briegleb, S. R. Jayne, M. Jochum, W. G. Large, S. Peacock, and S. G. Yeager, 2012: The CCSM4 ocean component. *J. Climate*, **25**, 1361–1389, doi:10.1175/JCLI-D-11-00091.1.

de las Heras, M. M., and R. Schlitzer, 1999: On the importance of intermediate water flows for the global ocean overturning. *J. Geophys. Res.*, **104**, 15 515–15 536, doi:10.1029/1999JC900102.

Dong, S., S. Garzoli, M. Baringer, C. Meinen, and G. Goni, 2009: Interannual variations in the Atlantic meridional overturning circulation and its relationship with the net northward heat transport in the South Atlantic. *Geophys. Res. Lett.*, **36**, L20606, doi:10.1029/2009GL039356.

——, M. Baringer, G. Goni, and S. Garzoli, 2011a: Importance of the assimilation of Argo float measurements on the meridional overturning circulation in the South Atlantic. *Geophys. Res. Lett.*, **38**, L18603, doi:10.1029/2011GL048982.

——, S. L. Garzoli, and M. O. Baringer, 2011b: The role of interocean exchanges on decadal variations of the meridional heat transport in the South Atlantic. *J. Phys. Oceanogr.*, **41**, 1498–1511, doi:10.1175/2011JPO4549.1.

——, M. O. Baringer, G. J. Goni, C. S. Meinen, and S. L. Garzoli, 2014: Seasonal variations in the South Atlantic meridional overturning circulation from observations and numerical models. *Geophys. Res. Lett.*, **41**, 4611–4618, doi:10.1002/2014GL060428.

——, G. Goni, and F. Bringas, 2015: Temporal variability of the South Atlantic meridional overturning circulation between 20°S and 35°S. *Geophys. Res. Lett.*, **42**, 7655–7662, doi:10.1002/2015GL065603.

Drévillon, M., L. Terray, P. Rogel, and C. Cassou, 2001: Midlatitude Atlantic SST influence on European winter climate variability in the NCEP reanalysis. *Climate Dyn.*, **18**, 331–344, doi:10.1007/s003820100178.

Eden, C., and J. Willebrand, 2001: Mechanism of interannual to decadal variability of the North Atlantic circulation. *J. Climate*, **14**, 2266–2280, doi:10.1175/1520-0442(2001)014<2266:MOITDV>2.0.CO;2.

Enfield, D. B., A. M. Mestas-Nuñez, and P. J. Trimble, 2001: The Atlantic multidecadal oscillation and its relation to rainfall and river flows in the continental U.S. *Geophys. Res. Lett.*, **28**, 2077–2080, doi:10.1029/2000GL012745.

Ferrari, R., J. C. McWilliams, V. M. Canuto, and M. Dubovikov, 2008: Parameterization of eddy fluxes near oceanic boundaries. *J. Climate*, **21**, 2770–2789, doi:10.1175/2007JCLI1510.1.

Findlater, J., 1969: A major low-level air current near the Indian Ocean during the northern summer. *Quart. J. Roy. Meteor. Soc.*, **95**, 362–380, doi:10.1002/qj.49709540409.

Frierson, D. M., and Coauthors, 2013: Contribution of ocean overturning circulation to tropical rainfall peak in the Northern Hemisphere. *Nat. Geosci.*, **6**, 940–944, doi:10.1038/ngeo1987.

Garzoli, S. L., and Z. Garraffo, 1989: Transports, frontal motions and eddies at the Brazil-Malvinas Currents Confluence. *Deep-Sea Res.*, **36A**, 681–703, doi:10.1016/0198-0149(89)90145-3.

——, and R. Matano, 2011: The South Atlantic and the Atlantic meridional overturning circulation. *Deep-Sea Res. II*, **58**, 1837–1847, doi:10.1016/j.dsr2.2010.10.063.

Goni, G. J., F. Bringas, and P. N. Di Nezio, 2011: Observed low frequency variability of the Brazil Current front. *J. Geophys. Res.*, **116**, C10037, doi:10.1029/2011JC007198.

Gordon, A. L., 1985: Indian-Atlantic transfer of thermocline water at the Agulhas retroflection. *Science*, **227**, 1030–1033, doi:10.1126/science.227.4690.1030.

Goswami, B. N., V. Krishnamurthy, and H. Annmalai, 1999: A broad-scale circulation index for the interannual variability of the Indian summer monsoon. *Quart. J. Roy. Meteor. Soc.*, **125**, 611–633, doi:10.1002/qj.49712555412.

Hawkins, E., and Coauthors, 2011: Bistability of the Atlantic overturning circulation in a global climate model and links to ocean freshwater transport. *Geophys. Res. Lett.*, **38**, L10605, doi:10.1029/2011GL047208.

Jochum, M., 2009: Impact of latitudinal variations in vertical diffusivity on climate simulations. *J. Geophys. Res.*, **114**, C01010, doi:10.1029/2008JC005030.

——, G. Danabasoglu, M. Holland, Y. O. Kwon, and W. Large, 2008: Ocean viscosity and climate. *J. Geophys. Res.*, **113**, C06017, doi:10.1029/2007JC004515.

Johns, W. E., and Coauthors, 2011: Continuous, array-based estimates of Atlantic Ocean heat transport at 26.5°N. *J. Climate*, **24**, 2429–2449, doi:10.1175/2010JCLI3997.1.

Kang, S. M., D. M. Frierson, and I. M. Held, 2009: The tropical response to extratropical thermal forcing in an idealized GCM: The importance of radiative feedbacks and convective parameterization. *J. Atmos. Sci.*, **66**, 2812–2827, doi:10.1175/2009JAS2924.1.

——, I. M. Held, and S.-P. Xie, 2014: Contrasting the tropical response to zonally asymmetric extratropical and tropical forcing. *Climate Dyn.*, **42**, 2033–2043, doi:10.1007/s00382-013-1863-0.

Kay, J., and Coauthors, 2015: The Community Earth System Model (CESM) Large Ensemble Project: A community resource for studying climate change in the presence of internal climate variability. *Bull. Amer. Meteor. Soc.*, **96**, 1333–1349, doi:10.1175/BAMS-D-13-00255.1.

Klinger, B. A., and J. Marotzke, 2000: Meridional heat transport by the subtropical cell. *J. Phys. Oceanogr.*, **30**, 696–705, doi:10.1175/1520-0485(2000)030<0696:MHTBTS>2.0.CO;2.

Knight, J. R., R. J. Allan, C. K. Folland, M. Vellinga, and M. E. Mann, 2005: A signature of persistent natural thermohaline circulation cycles in observed climate. *Geophys. Res. Lett.*, **32**, L20708, doi:10.1029/2005GL024233.

——, C. K. Folland, and A. A. Scaife, 2006: Climate impacts of the Atlantic multidecadal oscillation. *Geophys. Res. Lett.*, **33**, L17706, doi:10.1029/2006GL026242.

Kriegler, E., J. W. Hall, H. Held, R. Dawson, and H. J. Schellnhuber, 2009: Imprecise probability assessment of tipping points in the climate system. *Proc. Natl. Acad. Sci. USA*, **106**, 5041–5046, doi:10.1073/pnas.0809117106.

Kushnir, Y., W. A. Robinson, I. Bladé, N. M. J. Hall, S. Peng, and R. Sutton, 2002: Atmospheric GCM response to extratropical sst anomalies: Synthesis and evaluation. *J. Climate*, **15**, 2233–2256, doi:10.1175/1520-0442(2002)015<2233:AGRTES>2.0.CO;2.

Latif, M., K. Arpe, and E. Roeckner, 2000: Oceanic control of decadal North Atlantic sea level pressure variability in winter. *Geophys. Res. Lett.*, **27**, 727–730, doi:10.1029/1999GL002370.

——, and Coauthors, 2004: Reconstructing, monitoring, and predicting multidecadal-scale changes in the North Atlantic thermohaline circulation with sea surface temperature. *J. Climate*, **17**, 1605–1614, doi:10.1175/1520-0442(2004)017<1605:RMAPMC>2.0.CO;2.

——, M. Collins, H. Pohlmann, and N. Keenlyside, 2006: A review of predictability studies of Atlantic sector climate on decadal time scales. *J. Climate*, **19**, 5971–5987, doi:10.1175/JCLI3945.1.

Lee, J.-Y., B. Wang, K.-H. Seo, J.-S. Kug, Y.-S. Choi, Y. Kosaka, and K.-J. Ha, 2014: Future change of Northern Hemisphere summer tropical–extratropical teleconnection in CMIP5 models. *J. Climate*, **27**, 3643–3664, doi:10.1175/JCLI-D-13-00261.1.

Lee, S.-K., and C. Wang, 2010: Delayed advective oscillation of the Atlantic thermohaline circulation. *J. Climate*, **23**, 1254–1261, doi:10.1175/2009JCLI3339.1.

——, W. Park, E. van Sebille, M. O. Baringer, C. Wang, D. B. Enfield, S. G. Yeager, and B. P. Kirtman, 2011: What caused the significant increase in Atlantic Ocean heat content since the mid-20th century? *Geophys. Res. Lett.*, **38**, L17607, doi:10.1029/2011GL048856.

——, C. R. Mechoso, C. Wang, and J. D. Neelin, 2013: Interhemispheric influence of the northern summer monsoons on the southern subtropical anticyclones. *J. Climate*, **26**, 10 193–10 204, doi:10.1175/JCLI-D-13-00106.1.

Lenton, T. M., R. J. Myerscough, R. Marsh, V. N. Livina, A. R. Price, and S. J. Cox, 2009: Using GENIE to study a tipping point in the climate system. *Philos. Trans. Roy. Soc. London*, **367A**, 871–884, doi:10.1098/rsta.2008.0171.

Li, C., and M. Yanai, 1996: The onset and interannual variability of the Asian summer monsoon in relation to land–sea thermal contrast. *J. Climate*, **9**, 358–375, doi:10.1175/1520-0442(1996)009<0358:TOAIVO>2.0.CO;2.

Lumpkin, R., and K. Speer, 2007: Global ocean meridional overturning. *J. Phys. Oceanogr.*, **37**, 2550–2562, doi:10.1175/JPO3130.1.

Manabe, S., and R. J. Stouffer, 1988: Two stable equilibria of a coupled ocean–atmosphere model. *J. Climate*, **1**, 841–866, doi:10.1175/1520-0442(1988)001<0841:TSEOAC>2.0.CO;2.

McPhaden, M. J., and D. Zhang, 2002: Slowdown of the meridional overturning circulation in the upper Pacific Ocean. *Nature*, **415**, 603–608, doi:10.1038/415603a.

——, and ——, 2004: Pacific Ocean circulation rebounds. *Geophys. Res. Lett.*, **31**, L18301, doi:10.1029/2004GL020727.

Medhaug, I., H. R. Langehaug, T. Eldevik, T. Furevik, and M. Bentsen, 2012: Mechanisms for decadal scale variability in a simulated Atlantic meridional overturning circulation. *Climate Dyn.*, **39**, 77–93, doi:10.1007/s00382-011-1124-z.

Neale, R. B., J. H. Richter, and M. Jochum, 2008: The impact of convection on ENSO: From a delayed oscillator to a series of events. *J. Climate*, **21**, 5904–5924, doi:10.1175/2008JCLI2244.1.

Peings, Y., and G. Magnusdottir, 2014: Forcing of the wintertime atmospheric circulation by the multidecadal fluctuations of the North Atlantic Ocean. *Environ. Res. Lett.*, **9**, 034018, doi:10.1088/1748-9326/9/3/034018.

Rodwell, M. J., and C. K. Folland, 2003: Atlantic air–sea interaction and model validation. *Ann. Geophys.*, **46**, 47–56, doi:10.4401/ag-3388.

Saunders, P. M., and B. A. King, 1995: Oceanic fluxes on the WOCE A11 section. *J. Phys. Oceanogr.*, **25**, 1942–1958, doi:10.1175/1520-0485(1995)025<1942:OFOTWA>2.0.CO;2.

Sloyan, B. M., and S. R. Rintoul, 2001: The Southern Ocean limb of the global deep overturning circulation. *J. Phys. Oceanogr.*, **31**, 143–173, doi:10.1175/1520-0485(2001)031<0143:TSOLOT>2.0.CO;2.

Sperber, K. R., H. Annamalai, I.-S. Kang, A. Kitoh, A. Moise, A. Turner, B. Wang, and T. Zhou, 2013: The Asian summer monsoon: An intercomparison of CMIP5 vs. CMIP3 simulations of the late 20th century. *Climate Dyn.*, **41**, 2711–2744, doi:10.1007/s00382-012-1607-6.

Stommel, H., 1961: Thermohaline convection with two stable regimes of flow. *Tellus*, **13**, 224–230, doi:10.1111/j.2153-3490.1961.tb00079.x.

Stouffer, R. J., and Coauthors, 2006: Investigating the causes of the response of the thermohaline circulation to past and future climate changes. *J. Climate*, **19**, 1365–1387, doi:10.1175/JCLI3689.1.

Sun, C., J. Li, F.-F. Jin, and R. Ding, 2013: Sea surface temperature inter-hemispheric dipole and its relation to tropical precipitation. *Environ. Res. Lett.*, **8**, 044006, doi:10.1088/1748-9326/8/4/044006.

——, ——, J. Feng, and F. Xie, 2015a: A decadal-scale teleconnection between the North Atlantic Oscillation and subtropical eastern Australian rainfall. *J. Climate*, **28**, 1074–1092, doi:10.1175/JCLI-D-14-00372.1.

——, ——, and F.-F. Jin, 2015b: A delayed oscillator model for the quasi-periodic multidecadal variability of the NAO. *Climate Dyn.*, **45**, 2083–2099, doi:10.1007/s00382-014-2459-z.

Sutton, R. T., and D. L. Hodson, 2005: Atlantic Ocean forcing of North American and European summer climate. *Science*, **309**, 115–118, doi:10.1126/science.1109496.

Talley, L. D., 2003: Shallow, intermediate, and deep overturning components of the global heat budget. *J. Phys. Oceanogr.*, **33**, 530–560, doi:10.1175/1520-0485(2003)033<0530:SIADOC>2.0.CO;2.

Ting, M., Y. Kushnir, R. Seager, and C. Li, 2011: Robust features of Atlantic multi-decadal variability and its climate impacts. *Geophys. Res. Lett.*, **38**, L17705, doi:10.1029/2011GL048712.

Trenberth, K. E., and J. M. Caron, 2001: Estimates of meridional atmosphere and ocean heat transports. *J. Climate*,

14, 3433–3443, doi:10.1175/1520-0442(2001)014<3433:EOMAAO>2.0.CO;2.

Tung, K.-K., and J. Zhou, 2013: Using data to attribute episodes of warming and cooling in instrumental records. *Proc. Natl. Acad. Sci. USA*, **110**, 2058–2063, doi:10.1073/pnas.1212471110.

Wang, B., and Z. Fan, 1999: Choice of South Asian summer monsoon indices. *Bull. Amer. Meteor. Soc.*, **80**, 629–638, doi:10.1175/1520-0477(1999)080<0629:COSASM>2.0.CO;2.

——, J. Liu, H.-J. Kim, P. J. Webster, S.-Y. Yim, and B. Xiang, 2013: Northern Hemisphere summer monsoon intensified by mega-El Niño/Southern Oscillation and Atlantic multidecadal oscillation. *Proc. Natl. Acad. Sci. USA*, **110**, 5347–5352, doi:10.1073/pnas.1219405110.

Wang, H., B. Wang, F. Huang, Q. Ding, and J. Y. Lee, 2012: Interdecadal change of the boreal summer circumglobal teleconnection (1958–2010). *Geophys. Res. Lett.*, **39**, L12704, doi:10.1029/2012GL052371.

Webster, P. J., and S. Yang, 1992: Monsoon and ENSO: Selectively interactive systems. *Quart. J. Roy. Meteor. Soc.*, **118**, 877–926, doi:10.1002/qj.49711850705.

——, V. O. Magana, T. Palmer, J. Shukla, R. Tomas, M. U. Yanai, and T. Yasunari, 1998: Monsoons: Processes, predictability, and the prospects for prediction. *J. Geophys. Res.*, **103**, 14 451–14 510, doi:10.1029/97JC02719.

Weijer, W., and Coauthors, 2012: The Southern Ocean and its climate in CCSM4. *J. Climate*, **25**, 2652–2675, doi:10.1175/JCLI-D-11-00302.1.

Yim, S.-Y., B. Wang, J. Liu, and Z. Wu, 2014: A comparison of regional monsoon variability using monsoon indices. *Climate Dyn.*, **43**, 1423–1437, doi:10.1007/s00382-013-1956-9.

Yoshimori, M., and A. J. Broccoli, 2008: Equilibrium response of an atmosphere–mixed layer ocean model to different radiative forcing agents: Global and zonal mean response. *J. Climate*, **21**, 4399–4423, doi:10.1175/2008JCLI2172.1.

Zhang, L., and C. Wang, 2013: Multidecadal North Atlantic sea surface temperature and Atlantic meridional overturning circulation variability in CMIP5 historical simulations. *J. Geophys. Res. Oceans*, **118**, 5772–5791, doi:10.1002/jgrc.20390.

Zhang, R., and T. L. Delworth, 2005: Simulated tropical response to a substantial weakening of the Atlantic thermohaline circulation. *J. Climate*, **18**, 1853–1860, doi:10.1175/JCLI3460.1.

——, and ——, 2006: Impact of Atlantic multidecadal oscillations on India/Sahel rainfall and Atlantic hurricanes. *Geophys. Res. Lett.*, **33**, L17712, doi:10.1029/2006GL026267.